Charles University in Prague
Faculty of Mathematics and Physics

MASTER'S THESIS

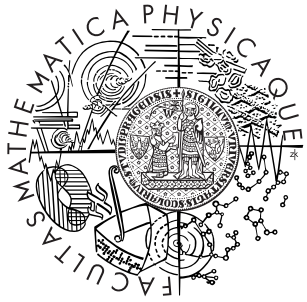

David Schmoranzer

Vibrating Quartz Crystal as a Tool for Studying the Flow of Cryogenic Fluids

Department of Low Temperature Physics

Thesis Supervisor: Professor RNDr. Ladislav Skrbek, DrSc.

Field of Study: Solid State Physics

This work is dedicated to all those who strive for a better understanding of this world through the means of science or otherwise.

First and foremost I would like to thank my parents, who have taught me to believe and to question. Further, my thanks also belong to all my friends, who have shown their support during the completion of this Thesis and in other times of need. Finally, I would like to express my deepest gratitude to my supervisor, Professor Ladislav Skrbek, for his friendly approach to students, his patience, and his priceless advice; to my laboratory colleagues Michaela Blažková and Tymofyi Chagovets for their invaluable help during the experiments and data processing and to all other students of physics who took part in the tremendous amount of work on this topic.

I hereby declare, that I have compiled my Master's Thesis alone and using only the cited references. I agree with allowing this Thesis to be lent.

In Prague dated 10th August, 2007 David Schmoranzer

Contents

Název práce: Vibrující křemenný krystal jako nástroj pro studium proudění kryokapalin
Autor: David Schmoranzer
Katedra: Katedra fyziky nízkých teplot
Vedoucí diplomové práce: Prof. RNDr. Ladislav Skrbek, DrSc.
e-mail vedoucího: skrbek@fzu.cz

Abstrakt: Tato práce se zabývá mnohostranným použitím komerčně dostupných křemenných ladiček při studiu dynamiky kryokapalin. Tyto křemenné krystaly se vyrábějí jako frekvenční standard do digitálních hodinek a vykazují značnou citlivost vzhledem k proudění okolního prostředí. V lineárním (tedy laminárním) režimu je lze použít k měření teploty, tlaku, viskozity, či vlastností proudění zkoumané kapaliny. V nelineárním režimu pak generují a detekují turbulenci. Křemenné ladičky jsme používali zejména k detekci přechodu mezi režimem laminární a turbulentní odporové síly v plynném héliu, normálním kapalném He I a v supratekutém He II. Podařilo se předpovědět a experimentálně ověřit závislost kritické rychlosti, při které dochází k tomuto přechodu ve viskózních tekutinách, v rozsahu čtyřech dekád a ukázali jsme, že v tomto případě je kritická rychlost skutečně úměrná odmocnině součinu kinematické viskozity a frekvence kmitů. Provedením stejných experimentů v supratekutém héliu jsme získali důkaz o existenci dvou kritických rychlostí - pro normální složku, která se chová jako klasická viskózní kapalina a pro supratekutou složku, která na frekvenci nejspíše nezávisí. Navíc se v normálním kapalném i v supratekutém héliu podařilo pomocí křemenných ladiček detekovat kavitaci.

Klíčová slova: křemenná ladička, helium, supratekutost, turbulence, kavitace

Title: Vibrating Quartz Crystal as a Tool for Studying the Flow of Cryogenic Fluids
Author: David Schmoranzer
Department: Department of Low Temperature Physics
Supervisor: Prof. RNDr. Ladislav Skrbek, DrSc.
Supervisor's e-mail address: skrbek@fzu.cz

Abstract: Commercially available quartz tuning forks produced as frequency standards for digital watches are used as multipurpose tools for cryogenic flow dynamics, thanks to their sensitivity to probe the flow of surrounding fluids. In linear (i.e., laminar) regime they can be used as sensitive thermometers, pressure- or flow- meters. In non-linear regime, they can serve as generators and detectors of turbulence. In particular, these oscillating quartz crystals are used to detect the transition from laminar to turbulent drag regime in gaseous Helium, normal liquid He I and superfluid He II. The scaling law for the critical velocity of this transition in viscous fluids is predicted and verified experimentally over four orders of magnitude and it is shown that in this case, the critical velocity is indeed proportional to the square root of the product of the kinematic viscosity and the frequency of oscillations. By extending the experiments to superfluid Helium, evidence is presented of two critical velocities; one for the normal fluid that behaves as an ordinary viscous fluid and one for the superfluid that seems frequency independent. Additionally, the tuning forks are used to study cavitation in normal and superfluid Helium liquids.

Keywords: quartz tuning fork, Helium, superfluidity, turbulence, cavitation

Chapter 1

Introduction

Helium. Proton number 2, molecular mass 4.00 g/mol, electron configuration $1s^2$. This is the summary of the facts about the second most abundant element in the Universe that are available to most people as they are listed in every periodic table. Unfortunately, none of these facts can give us even the slightest idea of the wide variety of extremely unusual and fascinating properties that the isotopes of this seemingly simple noble gas can display.

In chemistry, we are usually taught that Helium is a noble gas which forms monatomic molecules and that it's presence was first discovered in the Sun's emission spectrum. If we are lucky, we also learn that two stable isotopes of Helium exist, namely ^{3}He and ^{4}He, whose nuclei consist of two protons accompanied by one or two additional neutrons respectively. However, most students never find out about the most intriguing phenomenon associated with Helium - superfluidity. Perhaps this is because Helium becomes superfluid only at extremely low temperatures, unattainable without specialised cryogenic equipment, or it is due to the fact, that the fundamental principles governing the behaviour of superfluid Helium are still far from being fully understood.

Since presenting the full array of extraordinary properties the Helium isotopes exhibit is well beyond the scope of this work, we will concentrate only on the flow properties of ^{4}He (further on, Helium and He will always refer to ^{4}He), and especially on the transition from laminar to turbulent flows in its gaseous, liquid (He I) and superfluid (He II) phases. As the title suggests, these properties will be studied using a tool called the quartz tuning fork, which will be introduced once we learn something about ^{4}He in general and after we become familiar with the basics of continuum hydrodynamics.

Chapter 2

Basic Properties of Cryogenic Helium

The principal aim of this Chapter is to provide the reader with a concise overview of the basic properties of the Helium gas and liquids. Due to spatial restrictions, the properties will not be derived from all the underlying laws but instead they will be presented "as is", stressing rather facts than equations. Further information including a thorough and rigorous calculation is available in the referenced literature.

At room temperature, He obeys the Maxwell-Boltzmann distribution, behaves like any other ordinary gas and nothing extraordinary happens. Interesting phenomena arise at low temperatures where the bosonic nature of He atoms becomes prominent. What is however interesting about the classical He gas and liquid, is its thermodynamic and hydrodynamic properties, namely the most important parameter of any flow experiment, the kinematic viscosity, which can be varied over orders of magnitude simply by changing temperature and pressure and can reach much lower values in liquid He than eg. in air or water. For tabulated values of various quantities describing cryogenic Helium including its viscosity, see [1].

If we have a close look at the phase diagram of Helium (Fig. 2.1), we will immediately notice two striking features which no other substance exhibits and which are therefore unique to Helium - first, there is no triple point and second, the transition to a superfluid phase. No matter how deep we cool liquid helium at pressures below 25 bar, it will never freeze and will stay liquid till the absolute zero, however at the temperature of about 2.17 K something very strange will happen.

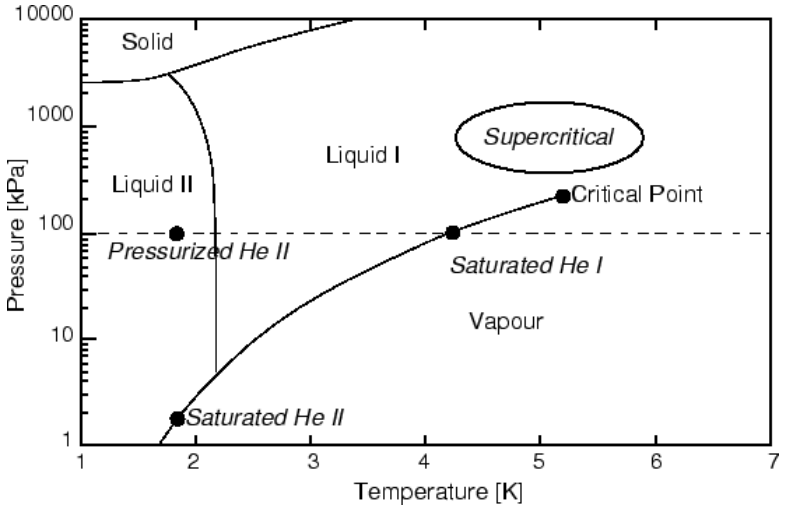

Figure 2.1: Phase diagram of ^{4}He

If we observed this cooling in a glass cryostat, we would notice that the violently moving level of the previously boiling helium suddenly forms a smooth surface (actually, with the precision of a monatomic layer, the smoothest natural surface ever). This could be explained by an extremely high heat conductivity and if we measured it, we would find that it is indeed at least six orders of magnitude larger than above this temperature. However, our greatest surprise would most likely be, that if we tried to measure the pressure drop in a He flow through a tiny orifice, we would find out that there is none at all, which would imply zero viscosity! This leads to the fact, that unlike normal viscous fluids, this He can flow even through infinitesimally small holes. Another surprising discovery would undoubtedly be the fact, that Helium below 2.17 K wets any substance except Cesium ideally, forming a thin film on its surface. The flow of this film can cause entire vessels of He to empty simply by passing over their walls. These are but a few of the variety of seemingly strange effects that take place in Helium below this temperature. But what really happens? Is there a theory which can explain them all?

What we know for sure is, that the event occurring at 2.17 K is a second order phase transition between normal He liquid (historically called He I) and so-called superfluid Helium (historically also called He II). It is fair to state, that despite the long time since the discovery of He II in the 1930's, there is still no microscopic theory today which would describe its behaviour in a

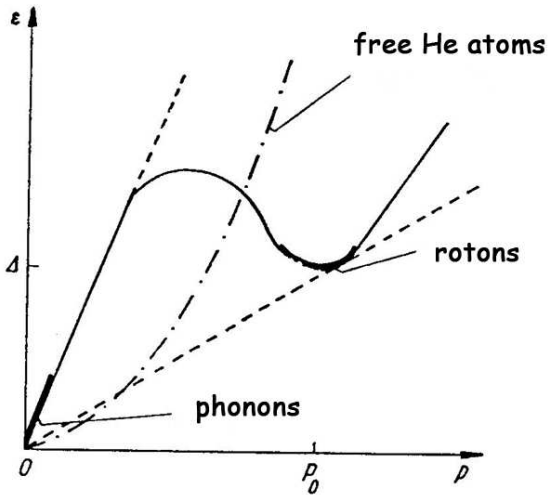

Figure 2.2: Landau model - Quasiparticle energy dispersion spectrum

comprehensive way. Not that we would not have enough theories, but either they are lacking accuracy of description or they just happen to be purely phenomenological. Two of these theories, specifically the Landau two-fluid model and Bose-Einstein condensation, will be introduced in greater detail, as their understanding will be necessary for further considerations.

2.1 Landau Two-Fluid Model

This phenomenological theory is based on the premise that He II can be described as an inseparable mixture of two constituents - the normal component, which behaves like classical fluids and the superfluid component, which has zero viscosity and entropy. Within the standard Landau model, these components do not interact. The sum of their densities correspond to the total density of He II and their ratio was first established from the famous Andronikashvili experiment (see Fig. 2.3) and later theoretically, following from the dispersion spectrum of quasiparticle excitations in He II (Fig. 2.2) which was first guessed by the famous Russian theoretician Landau and later proved by neutron diffraction. The relative densities depend solely on temperature and this dependence is illustrated in Fig. 2.3.

The standard two-fluid model is a very powerful tool for describing basic He II flow properties and wave processes, which can be derived solely based

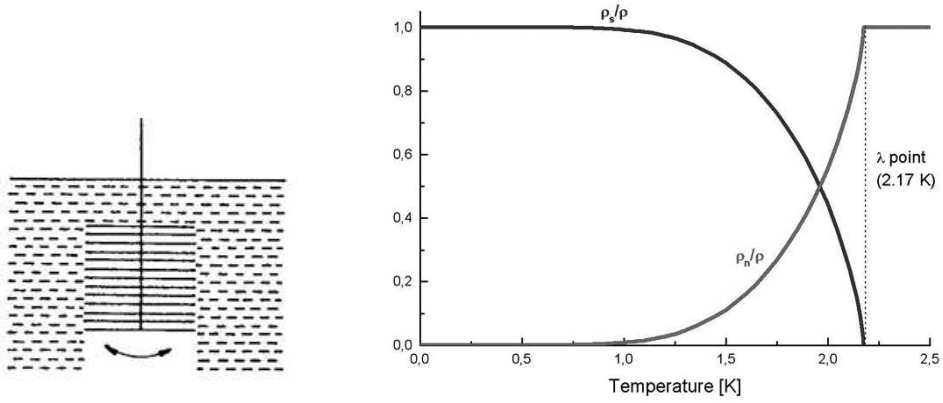

Figure 2.3: Stack of the discs used in the Andronikashvili experiment (schematics) and the relative densities of the normal and superfluid components

on the existence of the two independent components. Via this model, it is possible to explain the experiments mentioned above, such as apparent zero viscosity and it was even used to predict the existence of second sound in superfluid He (as is shown eg. in [2]), which is the core of several popular experimental techniques used today. One of the main achievements of this theory was also the prediction of a critical velocity at which excitations begin to be created and therefore superfluidity is destroyed, see also [2]. The two-fluid model also explains the fountain effect and its counterpart - the mechanocaloric effect (Fig. 2.4), even though these can be understood qualitatively in a simpler way by considering Bose-Einstein condensation.

There are, however, several phenomena, which cannot be explained by Landau's model unless additional assumptions are introduced. These include for example the existence of quantized vortices, the consequence of the collective behaviour of the Helium atoms which follows from Bose-Einstein condensation. We will therefore explore this theory based on statistical thermodynamics now.

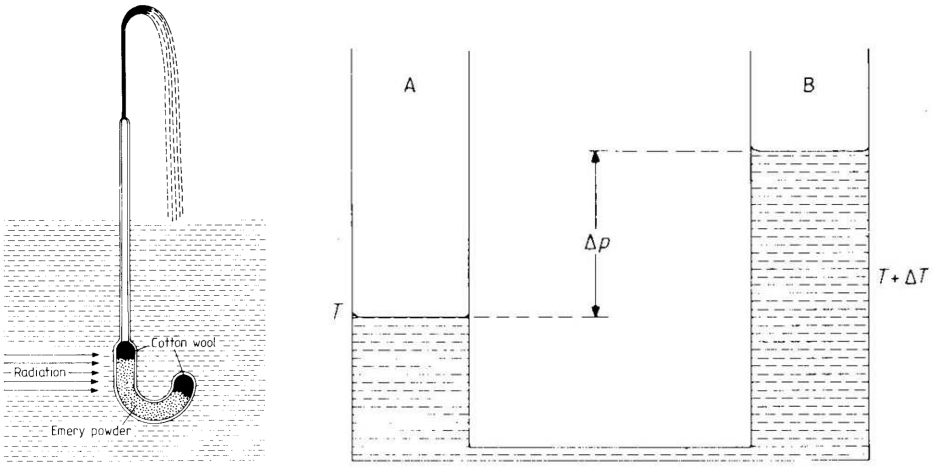

Figure 2.4: Fountain effect and the mechanocaloric effect

2.2 Bose-Einstein Condensation

All particles that form the matter in the universe can be divided into two groups based on their statistical behaviour in thermodynamic equilibrium. One of these groups is called fermions and these particles follow the Fermi-Dirac statistical distribution, while the other group is called bosons and they follow the Bose-Einstein distribution. It can also be shown from Quantum Field Theory that the spin of all bosons expressed in the units of the Planck constant is an integer, while the spin of fermions is always an integer + 1/2, the proof is however quite tedious and requires a deep understanding of QFT, but enthusiastic readers can find it in [3]. The two distributions governing the number of particles occupying a given energy state are expressed as follows:

$$n_i^{BE} = \frac{g_k}{e^{\frac{E_i-\mu}{k_B T}} - 1} \tag{2.1}$$

$$n_i^{FD} = \frac{g_k}{e^{\frac{E_i-\mu}{k_B T}} + 1} \tag{2.2}$$

The important point is, that at high enough temperatures or low enough concentrations (meaning $exp(E_i - \mu/k_B T) \gg 1$), both of these statistics reduce to the classical Maxwell-Boltzmann distribution and the behaviour of these two groups of particles is indistinguishable from the point of view

of statistical physics (though it of course still holds, that two fermions cannot occupy the same energy state, while two bosons can). Differences start to arise once we cool the system down to a temperature, which no longer satisfies the stated condition. If we have a bosonic system and reach the condensation temperature (derived eg. in [2]), the thermal De Broglie wavelength of the particles will become equal to the interparticle distances, the particles will start to behave collectively and to condense into the zero energy level. There is nothing to stop them from doing so because this simply minimizes the energy of the entire system. Fermions, however, cannot do anything similar because of an interaction, which is the basis of the Pauli exclusion principle, prohibiting two fermions to occupy the same energy state and therefore forcing them to occupy higher energy states as well. This leads to the creation of the Fermi sphere in the momentum space. The statistical behaviour of bosons and the condensation was discovered by Satyendra Nath Bose and Albert Einstein working together in the 1920's, therefore they bear their names. It is interesting to note, that the F-D distribution was discovered in 1926 by Fermi and Dirac working alone and independently which reflects the behaviour of the two types of particles beautifully.

Once we are below the condensation temperature, a macroscopic amount of the particles os the system will be in the zero energy level, while others will still remain in higher energy states. The existence of the Bose-Einstein condensate changes the thermodynamics of the entire system considerably. It can be shown [2] that if we consider a condensed ideal Bose gas as a thermodynamic system, its state will always be sufficiently described by a single quantity, eg. by temperature, and all of its other thermodynamic quantities e.g. pressure, volume and heat capacity will depend solely on this one selected parameter. Physically, even without calculations, this can be ascribed to the fact, that the ratio of particles in the condensate to the total number of particles becomes the only important parameter of the system, since all the particles in the condensate have the same energy (and therefore no thermodynamic degrees of freedom). Based on these simple considerations, it is already possible to predict the fountain effect and the mechanocaloric effect, as these are evident once we realize, that pressure will be a function of temperature only and therefore local heating will be equivalent to changing pressure locally thus creating a gradient.

Now we must ask, are there any links between the theory for the condensed ideal B-E gas and superfluid He II? The answer is not as simple as it might seem. The theoretical BEC critical temperature of Helium should be

about 3.15 K. The lambda transition in Helium occurs at 2.17 K at saturated vapour pressure. These two values are pretty close (within 50 percent), which hints that some links might be expected. However, liquid Helium is anything but a non-interacting gas, the interactions within Helium actually happen to be quite strong. Furthermore, if the condensate is supposed to have zero momentum, how can it flow? These and similar arguments were among the reasons why Landau himself in his lifetime never accepted this theory. The prediction and confirmation of the fountain effect and the mechanocaloric effect is however quite convincing, among dependencies deduced according to this theory such the temperature dependence of particles above the condensate or heat capacity. Today it is generally accepted, of course with the single exception, that it truly does not account for particle interactions. In the 1950's, Bogoliubov showed, that weak interactions can be taken into account as well.

2.3 Quantized Vorticity

As only a brief account, follows, the reader is directed to [4] for further information on quantum vortices. One of the most prominent features of the Bose-Einstein condensate is the collective behaviour of particles. This means, that using Quantum Mechanics, the condensate can be described by a macroscopic wave function:

$$\Psi(\vec{r},t) = \sqrt{\rho_s} e^{\imath\varphi(\vec{r},t)} \tag{2.3}$$

where the amplitude is given by the square root of the density of the condensate, ρ_s, and $\imath\varphi$ is the macroscopic phase. As well as with other QM wavefunctions, its square expresses the probability of finding a He atom in a certain volume, i.e. the density of Helium. We must however keep in mind, that this wavefunction describes the entire system, not just an individual particle, so that when we apply the momentum operator and divide by mass, we will obtain the actual flow velocity of the condensate (i.e., of the superfluid component of He II). Doing so, we get that the velocity is proportional to the gradient of the phase:

$$\vec{v}_S(r,t) = \frac{\hbar}{m_S} \nabla\varphi(r,t) \tag{2.4}$$

from which it follows, that the vorticity

$$\vec{\omega_S} = \nabla \times \vec{v_S} = \frac{\hbar}{m_S} \nabla \times \nabla\varphi(r,t) = 0 \tag{2.5}$$

of the superfluid component is zero. Now it would seem, that since the vorticity equals zero, the Stokes theorem yields that the circulation Γ defined as

$$\Gamma = \oint_C \vec{v_S} \cdot \vec{dl} = \int_S \vec{\omega_S} \cdot \vec{dS} \tag{2.6}$$

of the superfluid component must be zero as well, which would mean that there can be no rotational flows, not to mention turbulence. We do however recall, that many scientific works, including this Thesis, are actually dealing with the issue of superfluid turbulence, so there must be something more to it. Of course, the Stokes theorem only holds for simply connected areas, which is a condition that superfluid He actually manages to avoid. It creates quantized vortices, which do not have the superfluid component in their cores, and thus manufactures natural multiply connected areas in its volume, which can have non-zero circulation. If we express the circulation around such a vortex, we get

$$\Gamma = \oint_C \vec{v_S} \cdot \vec{dl} = \frac{\hbar}{m_S} \oint_C \nabla\varphi \cdot \vec{dS} = \frac{\hbar}{m_S} \triangle\varphi \tag{2.7}$$

As the wavefunction must be defined uniquely in space, it follows immediately, that the phase difference in the equation can only be equal to a multiple of 2π, which tells us, that circulation in the superfluid component is always quantized. Actually, since the energy of a vortex is proportional the number of carried circulation quanta squared [2], vortices having multiple quanta would be energetically unstable and thus all vortices carry exactly one quantum of circulation.

It should be stressed now, that this presents us with a prototype of turbulence, that is easier to describe than the turbulence in classical fluids, because in this case, all vortices differ only in the geometry of their cores, but otherwise, all of them are completely the same, which is a considerable simplification. Since the cores of vortices have the diameter of about 1 A, they can be modeled as lines in space, which enables many interesting numerical simulations of vortex dynamics unparalleled in classical fluids, because classical vortices lack the restraints imposed on their quantum counterparts.

Now, that we have explained the basic properties of superfluid Helium including two theories which attempt to describe them, we will carry on with

the introduction of the basic concepts of hydrodynamics, mostly regarding the general characteristics of laminar and turbulent flows and the transition between them. We will also introduce the equations of motion of fluids and the hydrodynamic model used to describe He II.

Chapter 3

Continuum Hydrodynamics in a Nutshell

In this chapter, we will briefly introduce the properties of laminar and turbulent flows including the criteria pertaining to the transition between them. We will proceed by revisiting the key steps of deriving the equations of motion of both ideal and viscous fluids, later modifying these equations to describe superfluid Helium within the framework of the Landau two-fluid model.

3.1 Laminar and Turbulent Flows

We will begin this section by analyzing a simple and yet important hydrodynamic experiment. Let us consider a flow of any viscous fluid, say water, through the horizontal pipe depicted in Fig. 3.1, which has three vertical branches next to a millimeter scale, which will provide information about local pressure. The first end of the pipe is connected to a container full of water, the other end is open and the pressure here will be equal to the atmospheric one. By adjusting the valve at the container, we will be able to control the flow velocity. The first thing we will notice is, that at low velocities, the water level in the three branches will be stationary, and that it will have a linear slightly decreasing tendency in the direction of the flow. This type of flow is called laminar. If we increase the velocity, we will eventually reach a region, where the water levels will no longer be stationary, which is a clear sign of local pressures and flow velocities varying in time and marking a transition region characteristic of the onset of turbulence. If we studied

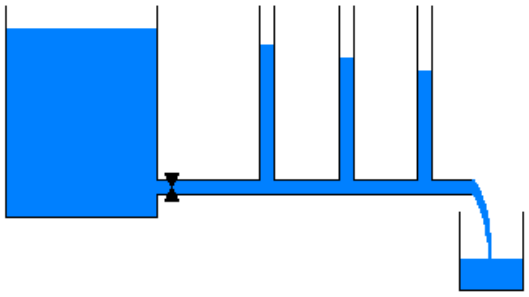

Figure 3.1: A typical experimental setup used to study the pipe flow

the average positions of the water levels, we would not be able to make any conclusions about the dissipative forces acting on the fluid, since the fluid will be switching between laminar and turbulent flow. If we increase the velocity further, the three water levels will still vary in time, but their average positions would now imply, that the pressure drop over a certain length of the pipe is much greater than in laminar flow. This is the case of fully developed turbulence.

This brief exercise serves only one purpose here - we need a description of laminar and turbulent flows, yet in any textbook, there are no definitions whatsoever! Not to be mistaken, there is a number of ways of characterizing laminar and turbulent flows but none of them can be used as a precise and rigorous definition (the reasons will be clearer once we derive the equations of motion and the Reynolds number). For now, we will therefore have to be content with stating several characteristics of each flow type, keeping in mind the example given above.

Laminar flows of viscous fluids are usually steady in time (or can be considered in a stationary approximation), which allows defining streamlines and the stream function, and in many cases they are also irrotational, which allows the introduction of a scalar flow potential, see [5]. The drag force acting on a body in a laminar flow is linear with the relative velocity of the body and the fluid. Turbulent flows are on the other hand characterised by abrupt changes of flow velocity in time and space, they are always rotational, consisting of intertwined vortices of many different length scales and the drag force acting on bodies experiencing turbulent flow is proportional to the velocity squared.

3.2 Equations of Motion of Fluids

We will now proceed by revising the most important ideas encountered during deriving the equations of motion of both ideal and viscous fluids. Since the following will be only a brief version of the derivation, the reader is directed to [5] or [6] for the full account.

First we shall introduce the concepts of continuum and of fluid particles. Even though, that every fluid must consist of individual molecules or atoms, this granularity of the fluid can be neglected at large enough length scales and high enough concentrations. From here it follows, that under normal circumstances, we can consider the fluid density a continuous function of space (neglecting individual particles) and use the continuum description. Since the behaviour of fluids is described by local differential equations, we will also need some infinitesimally small volumes where the equations will apply. We therefore introduce the idea of fluid particles, which are negligibly small compared to typical flow length scales, but at the same time are large enough not to be in contradiction with the continuum model. Now the description of fluid motion is reduced to describing the motion of a continuum of fluid particles.

The motion of fluid particles can be usually described in two different ways. The first possibility is to consider a given particle and watch its position and velocity in time and this is called the Lagrange description of fluids. The other possibility is obviously to watch a certain volume and analyze the velocity of any fluid particles currently in that volume. This other approach is called the Euler description of fluids and will be used throughout the rest of this Thesis.

3.2.1 Classical Fluids

Here, the equations governing the behaviour of classical fluids will be derived.

First, we will state the law of conservation of two quantities - mass and entropy. The first is known as the equation of continuity (3.1). The other one (3.2) is important only for thermally driven flows and is listed here only for the sake of completeness, as all the flows discussed herein can be considered isentropic. Both of the equations are expressed in the form typical of laws of conservation.

$$\frac{\partial \rho}{\partial t} + \nabla \cdot (\rho \vec{v}) = 0 \tag{3.1}$$

$$\frac{\partial(\rho S)}{\partial t} + \nabla \cdot (\rho S \vec{v}) = 0 \tag{3.2}$$

Within the bounds of applicability of classical physics, the motion of fluid particles must be determined by Newton's second law (equivalent to the conservation of momentum) and must therefore have the form of

$$\frac{D(\rho \vec{v})}{Dt} = \vec{F} \tag{3.3}$$

where $\frac{D}{Dt}$ signifies the change of the particle velocity in time (sometimes also the called material derivative). If we rewrite this equation using the Euler description, we obtain this form:

$$\frac{\partial \vec{v}}{\partial t} + (\vec{v} \cdot \nabla)\vec{v} = \frac{\vec{F}}{\rho} \tag{3.4}$$

Now, if we disregard any dissipative forces acting on the fluid and consider only the forces caused by the gradient of pressure within the fluid and gravity, we obtain the Euler equation for the motion of ideal fluids:

$$\frac{\partial \vec{v}}{\partial t} + (\vec{v} \cdot \nabla)\vec{v} = \frac{-\nabla p}{\rho} + g \tag{3.5}$$

If dissipative forces due to viscosity are included (we assume only Newtonian fluids, where viscosity can be reasonably defined) and gravity is neglected, as it has little effect in our case, we will obtain (see [5]) the infamous Navier-Stokes equation for isentropic incompressible flows, which has been troubling physicists and mathematicians since it very discovery:

$$\frac{\partial \vec{v}}{\partial t} + (\vec{v} \cdot \nabla)\vec{v} = \frac{-\nabla p}{\rho} + \nu \triangle \vec{v} \tag{3.6}$$

Equations 3.1, 3.2, and 3.6 together form a closed system sufficient to solve any incompressible flow of classical fluids, as they represent five equation for five quantities (three velocity components, pressure and entropy). However, since the N-S equation is a non-linear partial differential equation, it is possible to obtain an analytical solution only in a limited number of cases depending on the initial and boundary conditions including the flow geometry and flows in most practical applications have to be solved numerically.

3.2.2 Superfluid He II

Using the standard Landau two-fluid model, it is possible to obtain the equations governing the motion of superfluid helium. The equations are derived in a similar manner as for classical fluids, see, e.g., [2], the only difference being the existence of two components with independent densities and velocity fields, one of which has zero viscosity and entropy. The densities must obey:

$$\rho_n + \rho_s = \rho \tag{3.7}$$

Under the two-fluid model, the equation of continuity becomes:

$$\frac{\partial \rho}{\partial t} + \nabla \cdot (\rho_n \vec{v_n} + \rho_s \vec{v_s}) = 0 \tag{3.8}$$

Despite the fact, that the superfluid component carries no entropy, the law of conservation of entropy stays almost unmodified, since entropy S is defined per a unit of Helium liquid (not per a unit of the normal component), only the velocity is replaced by that of the normal component:

$$\frac{\partial (\rho S)}{\partial t} + \nabla \cdot (\rho S \vec{v_n}) = 0 \tag{3.9}$$

In He II, the behaviour of the normal component is determined by a Navier-Stokes type equation, while the inviscid superfluid component obeys a Euler type equation assuming no quantized vortices are present. In the case of incompressible isothermal (and therefore also isentropic) flow, these equations take the following form:

$$\frac{\partial \vec{v_n}}{\partial t} + (\vec{v_n} \cdot \nabla)\vec{v_n} = \frac{-\nabla p}{\rho} + \nu_n \triangle \vec{v_n} \tag{3.10}$$

$$\frac{\partial \vec{v_s}}{\partial t} + (\vec{v_s} \cdot \nabla)\vec{v_s} = \frac{-\nabla p}{\rho} \tag{3.11}$$

If a generalized two-fluid model is considered, where the two components of superfluid Helium interact, the interaction force is added as an extra term to the RHS of these equations. It can be shown [7], that the interaction force will be proportional to $\|\vec{v_n} - \vec{v_s}\|^3$ and can be therefore neglected at small counterflow velocities.

3.3 Geometrical Similarity, Transition to Turbulence

The Navier-Stokes equation mentioned above describes a very broad variety of flows in any Newtonian fluid. However, each rendition of the equation can be interpreted as a description not just of a single flow, but rather of a whole class of flows, which are geometrically similar. By geometrical similarity we understand what common sense tell us - that there is a scaling factor, which transforms one flow into the other precisely. However, if two different flow should reduce to the same N-S equations, this is not the only condition to be satisfied.

Focusing only on geometrically similar stationary flows now (thus avoiding temporal dependencies), we notice that a total of three quantities enters the N-S equation: a length scale, l, over which velocity changes appreciably and which enters implicitly via the spatial derivatives (typically the size of an immersed body or the radius of a pipe or container), the flow velocity, v, at a given point in space and the kinematic viscosity, ν, of the fluid. If all quantities in the N-S equation are replaced by their dimensionless counterparts:

$$l' = \frac{l}{l_0} \tag{3.12}$$

$$\vec{v'} = \frac{\vec{v}}{v_0} \tag{3.13}$$

$$\frac{p'}{\rho'} = \frac{p}{\rho}\frac{l_0}{v_0^2}, \tag{3.14}$$

it can be rearranged so that only one independent parameter remains:

$$(\vec{v}\cdot\nabla)\vec{v} + \frac{\nabla p}{\rho} = \frac{1}{Re}\triangle\vec{v} \tag{3.15}$$

For historical reasons, this parameter is called the Reynolds number and can be expressed as:

$$Re = \frac{lv}{\nu}, \tag{3.16}$$

where the scalar v is the magnitude of the velocity. It should be noted, that pressure (scaled by the fluid density) is not considered an independent

parameter, since it does not enter the N-S equation, but rather is obtained from it as a result. The N-S equation is of course complemented by the equation of continuity for incompressible steady flows, $\nabla \cdot \vec{v} = 0$, which already reduces the dimensionality of the problem from four to three unknowns.

Now it is clear, that if two different stationary geometrically similar flows have the same Reynolds number, they are described by the same N-S equation. Such flows are called *dynamically similar* as opposed to just *geometrically similar*.

A brief look at 3.15 tells us, that the ratio of the magnitudes of the inertial term plus the pressure gradient on the left to the viscous drag term on the right is in fact the Reynolds number. With bigger Reynolds numbers, the viscous term will be lower and the flow will have a greater tendency to become turbulent, as viscous forces represent the only mechanism preventing the onset of turbulence.

From here it follows, that once we have a given geometry of the flow, the transition between laminar and turbulent drag regimes will be defined solely by a certain critical value of the Reynolds number, Re_c, corresponding to a certain critical velocity, v_c. This is however true only for stationary flows. As we will be considering periodic flows due to an oscillating quartz crystal in this Thesis, it should be emphasized, that an additional condition must be satisfied in order for two flows to be dynamically similar, specifically, there is another dimensionless quantity that must be equal for both of the flows - the Strouhal number.

Named after the Czech physicist Čeněk Strouhal, who investigated the frequency of sound emitted by a wire moving rapidly through air, this number is derived from the typical time interval, τ, over which velocities change appreciably in the flow, e.g. from the period of oscillations or in the case of Strouhal's experiments, the period of creation of vortices behind the wire. It can be expressed as:

$$St = \frac{v\tau}{l}. \tag{3.17}$$

Finally, it should also be stressed, that the transition between linear and turbulent flows does not occur at precisely defined values of the Reynolds and Strouhal numbers, instead experimental evidence indicates, that a transition region occurs, where the flow is switching between both regimes, depending on the magnitude and frequency of various perturbations that break down the laminar flow.

Chapter 4

Quartz Tuning Forks

In this Chapter, we will introduce the sensor used in our experiments - the vibrating quartz tuning fork - and proceed to explain the hydrodynamic model used to describe its motion in fluids.

In the research of cryogenic liquids, oscillating objects have become almost traditional and certainly irreplacable tools for probing various types of flows. Starting more than fifty years ago, when Andronikashvili used an oscillating stack of closely spaced disks to measure the ratio of the densities of the normal and superfluid component of He II, various other oscillators found their use in cryogenic fluid dynamics (both in ^{3}He and ^{4}He), including vibrating spheres [8], reeds [9], grids [10],[11] and wires [12], [13], [14]. The quartz tuning fork presents a new and interesting addition to this family of oscillators, as its operation mode shows some important differences from other objects, mainly due to its comparatively high frequency, as will be discussed later.

Typical quartz tuning forks are commercially produced piezoelectric oscillators meant to be used as frequency standards in digital watches. At room temperature in vacuum, they oscillate at a calibrated standard frequency of 2^{15}Hz (= 32 768 Hz). However, the characteristics of individual forks differ in cryogenic conditions and therefore calibration is necessary. The forks are supplied in a vacuum-tight metal can, which has to be entirely or partly removed for any hydrodynamic applications. For a better idea of the forks appearance, see Fig. 4.1.

The quartz tuning fork offers several important advantages as a sensor of its cryogenic environment. Forks are extremely cheap and readily available, they are robust and as such easy to install and use if reasonable care is taken

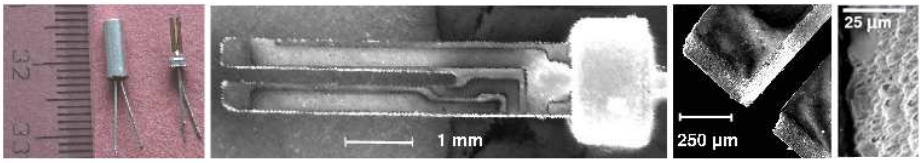

Figure 4.1: Photographs and micrographs of quartz tuning forks

during the manipulation. They are highly sensitive indicators of the physical properties of the medium in which they are immersed. A major advantage in many applications is that to drive these piezoelectric devices no magnetic fields are needed and that they are in fact insensitive to them.[15, 16]

In the experiments described herein, the forks were used as generators and detectors of both laminar and turbulent flows in cryogenic Helium depending on the amplitude of the driving voltage. The purpose is to obtain information about the transition between the two flow regimes and compare the results from all media available - from Helium gas, He I and He II. In order to understand, how the fork operates as a sensitive detector of its surroundings, a hydrodynamic model will be introduced, describing its behaviour when immersed in viscous fluids.

4.1 Hydrodynamic Model of the Tuning Fork

The aim of this section is to obtain the theoretical relations for the parameters of the resonance curve of the quartz oscillator depending on the density and viscosity of the medium in which it is immersed. For the sake of clarity, we will first discuss only the motion of the fork in vacuum and in the next step, the influence of the surrounding medium will be incorporated into our analysis as well.

At low amplitudes of oscillations, the fork can be considered as a damped harmonic oscillator driven by a harmonic force with the relevant oscillation mode being the basic antisymmetric mode, when the two prongs move in anti-phase. When considering vacuum, the damping arises only from the dissipation of energy through internal friction in the quartz crystal related to the motion of point defects, dislocations and other structures or processes disrupting the crystal lattice e.g. thermal motion of the atoms. We will assume this friction force to be approximately proportional to velocity, but

since it is much smaller than the friction force caused by any surrounding medium, the exact dependence is not really important. The equation of motion for a single prong of the fork has the following form:

$$m_0 \frac{d^2x}{dt^2} + \Gamma_0 \frac{dx}{dt} + kx = F_0 cos(\omega t), \tag{4.1}$$

where m_0 is the effective mass of the prong in vacuum, Γ_0 expresses the internal friction and k is the spring constant.

The solution to this equation is well known. It is found in the form of the Lorentzian absorption and dispersion curves and can be expressed as:

$$x_0(t) = x_{\mathrm{a0}}(\omega)\sin(\omega t) + x_{\mathrm{d0}}(\omega)\cos(\omega t), \tag{4.2}$$

where x_{d0} and x_{a0} are the dispersion and absorption, respectively. These curves have the following mathematical transcription:

$$x_{a0}(\omega) = x_0 \frac{\Gamma_0 \omega^2}{(\Gamma_0\omega)^2 + (m\omega^2 - k)^2} = \frac{x_0(\Delta\omega_0)^2\omega^2}{(\Delta\omega_0)^2\omega^2 + (\omega^2 - \omega_0^2)^2} \tag{4.3}$$

$$x_{d0}(\omega) = x_0 \frac{\omega(m\omega^2 - k)}{(\Gamma_0\omega)^2 + (m\omega^2 - k)^2} = \frac{x_0\Delta\omega_0\omega\,(\omega^2 - \omega_0^2)}{(\Delta\omega_0)^2\omega^2 + (\omega^2 - \omega_0^2)^2}, \tag{4.4}$$

where $\Delta\omega_0$ is the resonant linewidth of the fork in vacuum (i.e. the full width of the absorption curve at half of its maximum x_0).

The important result here is, that the resonant frequency $\omega_0 = (k/m_0)^{1/2}$ depends on the effective mass of the prong and that the resonant linewidth $\Delta\omega_0 = \Gamma_0/m_0$ depends on the effective mass as well and more importantly on size of the dissipative forces.

Now we are ready to discuss the effects of immersing the fork in a viscous medium. The classical viscous flow around a submerged oscillating body[5] is rotational within a certain layer adjacent to the body, while at larger distances it rapidly changes to potential flow if there is no free liquid surface or solid surface in the vicinity of the oscillating body. The depth of penetration of the rotational flow is of order

$$\delta = \sqrt{\frac{2\nu}{\omega}} = \sqrt{\frac{2\eta}{\rho\omega}}, \tag{4.5}$$

where ω is the angular frequency of oscillation while η and $\nu = \eta/\rho$ are the dynamic and kinematic viscosities of the fluid with the density ρ.

As a result of the oscillatory motion of the body through the liquid, the body experiences a force which has components proportional to the velocity of the body $\dot{x}$ (drag) and to its acceleration $\ddot{x}$ (mass enhancement):

$$F = \Gamma_1 \dot{x} + \tilde{m}\ddot{x}. \tag{4.6}$$

The new equation of motion including this force therefore is:

$$m\frac{d^2x}{dt^2} + \Gamma\frac{dx}{dt} + kx = F_0 cos(\omega t), \tag{4.7}$$

where $m = m_0 + \tilde{m}$ is the effective mass of the fork prong in the medium and $\Gamma = \Gamma_0 + \Gamma_1$ is the total friction experienced by the prong.

To determine the values of b and $\tilde{m}$ generally a full solution of the flow field around the oscillating body is required. However, in our case, a simplification is possible due to the ratio of the relative magnitudes of the characteristic size of the oscillating body l, oscillation amplitude x_0, and viscous penetration depth δ. Due to the high frequencies of oscillation and low kinematic viscosity of Helium, the penetration depth is very small (approx. $0.5\,\mu m$) and we are operating in the limit $l \gg \delta$ and $l \gg x_0$ as the oscillation amplitude would reach the leg thickness $\mathcal{T}$ only at very high velocities of several m/s. In this case the layer of rotational flow around the body is very thin, while in the rest of the fluid, the flow is potential. Note that other oscillating objects such as spheres or wires may not always be in this flow regime since they usually have smaller characteristic sizes and lower oscillation frequencies.

If these conditions are valid, a major contribution to both b and $\tilde{m}$ in Eq. (4.6) is found by solving the potential flow field u around the body.[5] In particular, b is expressed as

$$\Gamma_1 = \sqrt{\frac{\rho\eta\omega}{2}}\,\mathcal{C}\,S\ , \tag{4.8}$$

where S is the surface area of the body, and $\mathcal{C}$ is a numerical constant depending on the exact geometry of the body.

The largest contribution to mass enhancement $\tilde{m}$ arises from the potential flow around the body and can be expressed through the mass ρV of the liquid displaced by the body of volume V. A smaller contribution is caused by the fact that the viscous drag force experienced by the body is usually phase shifted with respect to the velocity of the body. This can be inter-

preted such that a volume of order $S\delta$ of the liquid is clamped to move with the oscillating body. Thus for $\tilde{m}$ we can write

$$\tilde{m} = \beta\rho V + B\rho S\delta \ , \tag{4.9}$$

where β and B are again geometry-dependent coefficients.

Though it is possible to obtain the exact values of β, B, and $\mathcal{C}$ for, e.g., spheres, cylinders oscillating perpendicularly to their axis or even beams, the author is not aware of any rigorous calculation of these parameters for a tuning fork. The results for beams cannot be used, as the presence of two prongs of the fork in close vicinity affects the flow significantly, changing for example the β parameter. We will therefore consider β, B, and $\mathcal{C}$ as fitting parameters, to be determined for a particular fork from the experiment. This approach was previously used, for example, in Ref. [9] for the description of the behavior of a vibrating reed in liquid ^{4}He and it proved to be a useful technique for the initial understanding of the experimental results.

To summarize the effects due to the viscous medium, we shall state, that we found the new effective mass of a prong as:

$$m = m_0 + \beta\rho V + B\rho S\delta \ , \tag{4.10}$$

and the new friction force as:

$$\Gamma = \Gamma_0 + \sqrt{\frac{\rho\eta\omega}{2}}\,\mathcal{C}\,S \ . \tag{4.11}$$

This information can be used to express the resonant frequency, f_m, and linewidth, Δf_m, as they will be modified by the presence of the medium, yielding the so called fork equations:

$$\left(\frac{f_0}{f_m}\right)^2 = 1 + \frac{\rho}{\rho_\mathrm{q}}\left(\beta + B\,\frac{S}{V}\sqrt{\frac{\eta}{\pi\rho f_m}}\right), \tag{4.12}$$

$$\Delta f_m = \left(\Delta f_0 + \frac{1}{2m_0}\sqrt{\frac{\rho\eta f_m}{\pi}}\,\mathcal{C}\,S\right)\left(\frac{f_m}{f_0}\right)^2, \tag{4.13}$$

where ρ_q is the density of quartz and the indices "0" and "m" denote the quantities related to vacuum and a viscous medium respectively.

Now we are familiar with the behaviour of the fork at low amplitudes of oscillation, but what happens, when the amplitude increases? It is found

experimentally and shown in Chapter 6 that at a certain amplitude, the response of the fork ceases to be of the Lorentzian form, which is caused by the fact, that the damping force due to the surrounding medium is no longer linear with velocity, but assumes a quadratic dependence instead, which corresponds to the transition from the laminar to turbulent drag regime within the fluid.

4.2 Electrical Properties of the Tuning Fork

In the previous section, we explored the behaviour of the quartz tuning fork as a mechanical oscillator. Here we will show that when the leads of the fork are connected to a harmonic driving voltage, an analogy exists between the mechanical oscillator and the electrical oscillatory circuit, which can be considered as a series RLC resonator in the first approximation.

The first relation between the two resonators arises from the piezoelectric effect and states that stresses in the piezoelectric crystal caused by its deflection induce electrical charges or that the current flowing through the crystal is proportional to the time derivative of the deflection, i.e. the velocity:

$$I(t) = a\,\frac{dx(t)}{dt}\ , \tag{4.14}$$

where a is the fork constant. Its theoretical value is given by [17] as

$$a = 3\,d_{11}\,E\,(\mathcal{T}\,\mathcal{W}/\mathcal{L})\ , \tag{4.15}$$

where d_{11} and E are the longitudinal piezoelectric modulus and the the Young modulus of quartz respectively. Here, $\mathcal{T}$, $\mathcal{W}$ and $\mathcal{L}$ stand for the thickness, width and length of a fork prong, respectively.

Furthermore, the current flowing through a series RLC oscillatory circuit obeys the following differential equation:

$$L\frac{d^2I}{dt^2} + R\frac{dI}{dt} + \frac{I}{C} = \frac{dU}{dt}\ . \tag{4.16}$$

Comparing Eqs. (4.16) and (4.7) we see that $\omega_0^2 = 1/(LC)$, $\Gamma/m = R/L$, and using Eq. (4.14), $1/L = (F_0/U_0)\,a/m$. Additionally we have the condition that the dissipated power at resonance has to be equal for both equations: The electrical power $U_0^2/(2R)$ drives two legs of the fork which dissipate $2 \cdot F_0^2/(2\Gamma)$. Thus we have a closed set of equations allowing us

to connect the electrical and mechanical properties of the fork via the fork constant a:

$$\begin{aligned} F_0 &= (a/2)\, U_0 \ , && (4.17)\\ R &= 2\Gamma/a^2 \ , && (4.18)\\ L &= 2m/a^2 \ , && (4.19)\\ C &= a^2/(2k) \ . && (4.20) \end{aligned}$$

Experimentally the fork constant a can be determined using Eq. (4.18), which can be rewritten as

$$a = \sqrt{\frac{2m\,\Delta\omega}{R}} \ . \tag{4.21}$$

Here $\Delta\omega$ is determined from the width of the resonance curve while $1/R$ is the linear slope of the experimental $I_0(U_0)$ dependence, where I_0 is the current amplitude at resonance. This measurement of course has to be taken in vacuum at the temperature of the planned hydrodynamic experiment.

4.3 Theoretical Predictions

The first thing that has to be done before any actual measurements is the verification of the hydrodynamic model used. For this purpose, we will use the fork equations to derive the dependence of the resonant frequency and linewidth of the fork on the pressure of a surrounding ideal gas. This dependence will later be verified in Helium and Nitrogen at room temperature.

First, we will neglect the second term in the bracket in Equation 4.12 as it can be shown to be significantly lower than the first one (both β and B are of order unity, the S/V ratio is $\ll 1$ and using the data for Helium and Nitrogen, the square root is also less then 1). This yields:

$$f_m = f_0 \frac{1}{\sqrt{1 + \frac{\rho}{\rho_q}\beta}}, \tag{4.22}$$

and since the densities of the gases at pressures achievable within our cell are much lower then the density of quartz, $\rho \ll \rho_q$, the final approximative dependence can be expressed as follows:

$$f_m = f_0(1 - \frac{\rho}{2\rho_q}\beta). \tag{4.23}$$

As the density of an ideal gas is directly proportional to its pressure, we therefore expect to find the resonant frequency decreasing linearly as the pressure is increased, however, the relative change in the frequency for pressures up to 30 bar will be quite negligible, again because of the ratio of the respective densities.

Repeating a similar process with the linewidth, where we neglect the ratio $(f_m/f_0)^2$ and replace f_m by f_0 under the square root due to reasons explained in the previous paraFig., we obtain:

$$\Delta f_m = \Delta f_0 + \frac{1}{2m_0}\sqrt{\frac{\rho\eta f_0}{\pi}}\,\mathcal{C}\,S. \tag{4.24}$$

Bearing in mind, that the dynamic viscosity, η, of an ideal gas is by definition independent of pressure, we arrive at a conclusion, that the linewidth will be proportional to the square root of the pressure and shifted by its vacuum value Δf_0.

For liquid Helium, similar reasoning can be applied regarding the resonant frequency except that the density is no longer directly proportional to the pressure. Regarding the linewidth, the actual values of dynamic viscosity have to be taken into account in order to obtain a reasonable dependence.

However, another, and perhaps the most important prediction for liquid Helium follows from the relative magnitudes of the viscous penetration depth, δ, the typical dimension of the fork, l. For the relevant frequencies of the order $3 \cdot 10^4$, $\delta \approx 0.5\mu m$ while the smallest dimensions of the fork are several hundreds of μm.

Since $\delta \ll l$, it becomes apparent, that the relevant length scale used in the computation of the Reynolds and Strouhal numbers will not be the dimension of the fork, but the viscous penetration depth itself. Substituting δ as expressed in Eq. 4.5 into equations 3.16 and 3.17 and replacing the time interval τ by $2\pi/\omega$ by we obtain:

$$St = \pi Re = \sqrt{2}\frac{v}{\sqrt{\nu\omega}}, \tag{4.25}$$

which tells us two interesting facts: first, any one of these numbers is sufficient for determining the dynamical similarity of flows including the transition to turbulence, as they differ only by a multiplicative constant and

second, if the transition occurs at a given value of the, say, Reynolds number, the critical velocity, v_c, at which the transition occurs, should scale as $\sqrt{\nu\omega}$. While this scaling law for oscillating objects may seem rather obvious, still it was never verified experimentally, possibly due to the lack of suitable oscillators operating at high enough frequencies.

To strengthen this claim, the same scaling can be derived analytically by equating the laminar and turbulent drag forces acting on an immersed body vibrating in a fluid. We will illustrate this on the analytically tractable example of an oscillating sphere. For $R \gg \delta$ and according to [5], the laminar and turbulent drag forces acting on such a sphere are equal to:

$$F_{lam} = \left[6\pi\eta R v \left(1 + \frac{R}{\delta}\right)\right]_{R \gg \delta} \approx 6\pi\eta R^2 v, \tag{4.26}$$

$$F_{turb} = \frac{1}{2} C_d \rho R^2 v^2. \tag{4.27}$$

By putting $F_{lam} = F_{turb}$, the critical velocity of the transition between the laminar and turbulent drag regimes is obtained as:

$$v_c = \frac{12}{C_d}\sqrt{\frac{\nu\omega}{2}}, \tag{4.28}$$

which is in accordance with the proposed scaling.

Chapter 5

Experimental Setup

In this Chapter, the experimental setup used during the work on this Thesis as well as during other experiments will be introduced. We will begin by a brief description of the used apparatus and measurement instrumentation and then we will proceed to the used software and describe the experimental protocol.

5.1 Hardware

The most important piece in the whole setup is undoubtedly the quartz tuning fork itself. Actually, various types of forks were used during these experiments ranging from the smallest oscillating at ≈ 32 kHz to the largest fork oscillating at ≈ 4 kHz (5.1), most experiments were however performed using one of the two sizes of forks that oscillate at 32 kHz since these can be easily fitted into a small pressure cell. The other forks were used in an open bath.

The home-made pressure cell (depicted in Fig 5.2) is Indium-sealed and withstands safely pressures up to 30 bar. During the experiments, it is placed inside a glass cryostat (Fig. 5.3) and it is filled by the desired fluid via a capillary connected to a piping panel through a cold trap. The purpose of the cold trap is to remove any possible frozen impurities in technical Helium that might otherwise block the capillary or settle down on the fork, thus reducing its sensitivity and devaluating the information obtained from the characteristics of its response.

Two pressure meters are used, a analogue Leybold–Heraeus and a digital Barotron, to measure the pressure inside the cell or inside the cryo-

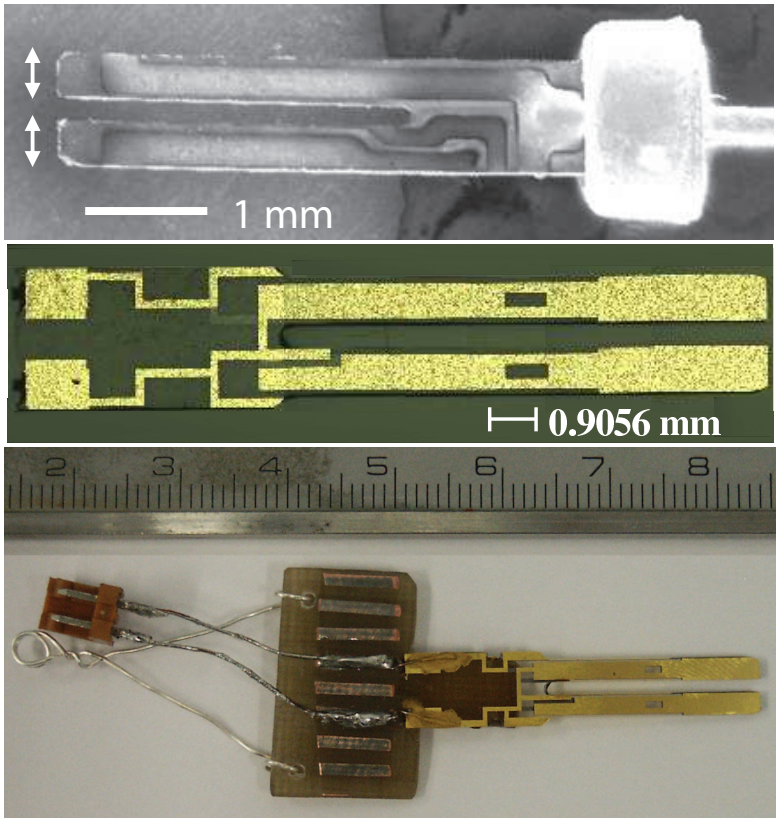

Figure 5.1: Top to bottom: Details of the 32 kHz, 8 kHz, and 4 kHz fork

stat. Measuring the pressure in the cryostat allows determining the temperature of the Helium bath, since if care is taken not to manipulate the pressure/temperature quickly, Helium exists in the cryostat at saturated vapour pressure.

The cryostat used is a standard glass cryostat provided with a shielding Nitrogen bath, separated from the Helium bath by evacuated space. The Helium bath itself is also covered by a reflective layer of silver reducing incoming radiation with only a narrow viewport allowing visual observation of the experiment. Using a Roots pump to reduce the pressure above the Helium level, the temperature can be reduced as low as $1.2 - 1.3$ K in this cryostat.

As for the electronics, the necessary equipment includes an Agilent signal generator providing the driving voltage of the fork, a step-up transformer and an attenuator, which allow us to shift the operating range of the gen-

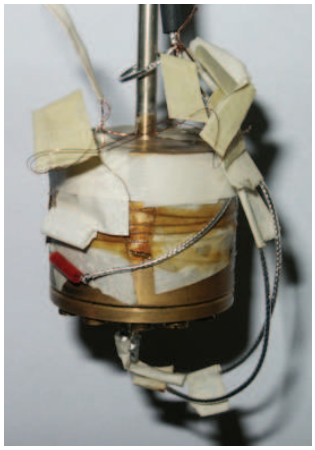

Figure 5.2: The pressure cell used in our experiments where two forks can be installed filled by Helium - working fluid - via the capillary that enters the cell inside the supporting stainless steel tube on the top. Special cryogenic stainless steel coaxial cables used to drive and readout the forks can be seen as well.

erator to either higher or lower values, a home-made current splitter and a commercial lock-in amplifier SR 830, which is a detector of the fork's response, measuring the amplitude of both the absorption (in-phase) and dispersion (out-of-phase) signals with an extremely high resolution and sensitivity. An optional device to this experiment is a Conductus temperature controller, which provides better thermal stability of the system should it be needed, but most of the experiments were performed without operating it, as the thermal stability was usually satisfactory once the fluctuations of the system relaxed. See the connection diagram in Fig. 5.4 for a better understanding of the electrical circuit used for driving the fork and reading its response.

The generator, the SR 830 lock-in amplifier, the Barotron pressure meter and the Conductus temperature controller were connected to a PC using the GPIB bus, which provided a handy way of controlling the experiment and reading the acquired data.

5.2 Software and Experimental Protocol

The controlling software was programmed in the LabView 7.1 Fig.ical programming environment. Its principal features allowed sweeping the frequency across the resonance in a defined manner and reading the measured reso-

Figure 5.3: The laboatory glass cryostat

nance curves. The absorption signal was fitted by its analytical function and the resonant frequency, linewidth and amplitude were evaluated. The data was recorded into files for further processing using the Origin 7.0 software.

During the experiments, several important rules had to be kept in mind. First, the purity of the fluid was essential, especially liquid Helium. Therefore, if experiments at varied pressures were performed, they always had to start at the highest pressure and then proceed gradually to the lower ones. This ensured that during the experiments Helium flowed only in the direction out of the pressure cell, preventing any impurities from reaching the fork.

Second, thermal stability had to be ensured. If temperatures were changed during the experiments, i.e., by adjusting the rate of outgoing Helium gas, it

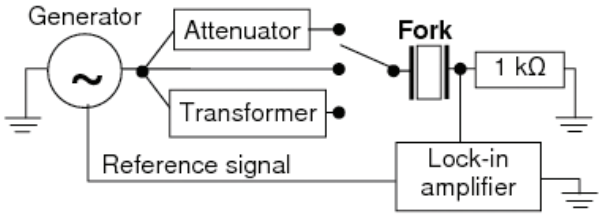

Figure 5.4: Fork connection diagram

was necessary to wait for approx. 20 minutes before new experiments could be performed. The thermal stability was verified by monitoring the fork's response and/or the temperature controller.

Third, temporal stability. If a mechanical oscillator is switched on, or if its frequency is changed suddenly, its response approaches the new value exponentially with the decay time equal to $1/\Delta\omega$ s. Thus, since the frequency of the driving voltage is swept across a certain range, sufficient time (about $4/\Delta\omega$ s) had to be provided for the fork to assume each new frequency. Fulfilling this requirement could be verified by sweeping the frequency upwards and downwards for the same conditions and comparing the shape of the response curves.

Chapter 6

Results and Discussion

In this Chapter, the main results acquired during the measurements performed on the quartz tuning forks will be presented and their possible implications on the nature of flow properties of cryogenic Helium will be discussed.

All the results were obtained in the Joint Low Temperature Laboratory established between the Faculty of Mathematics and Physics of the Charles University in Prague and the Physics Institute of Physics of the Academy of Sciences of the Czech Republic. Most of them have already been published in several papers [18], [19], [20] and presented at various conferences including QFS Kyoto 2006 and QFS Kazan 2007. The author of this Thesis contributed mostly by performing selected experiments and processing their output either individually or in cooperation with other laboratory colleagues.

The principal aim of the performed experiments was to generate and detect laminar and turbulent flows in both classical and superfluid Helium using the quartz tuning fork and to establish the criteria for the transition to turbulence. To make this possible, several key steps had to be completed first.

The first step was obviously the verification of the hydrodynamic model proposed in Chapter 4. In order to test the model, the fork was first mounted into the pressure cell, and immersed in gaseous nitrogen and helium at room temperature. Then it was excited at a low amplitude of the driving voltage in order to ensure that it operated in the linear regime and the resonant frequency and linewidth were measured for different pressures up to 30 bar and compared to the expected dependencies. The results of this verification are shown in Fig. 6.1.

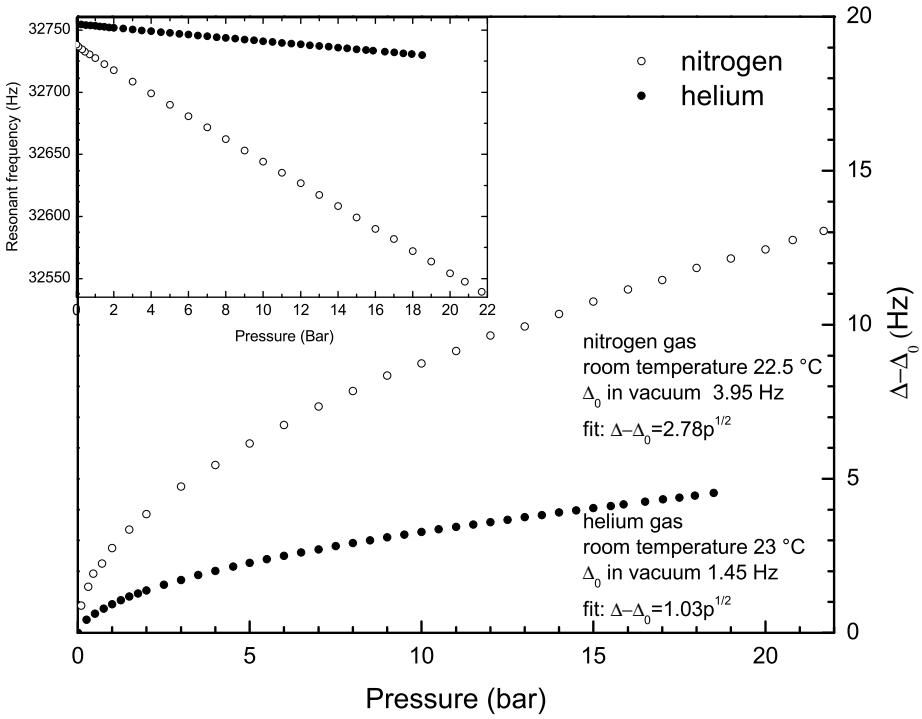

Figure 6.1: Pressure dependence of resonant frequency and linewidth measured with the standard 32 kHz fork in N_2 and He gases at room temperature

As it is apparent from the figures, the resonant frequency indeed behaves according to the prediction 4.23 based on our model. It decreases linearly with increasing pressure, however, its relative change tends to be rather small at the given pressures. The linewidth follows the prediction of Eq. 4.24 too, as its dependence on the applied pressure is of the square root form. The fitted lines were used to determine the values of the parameters β and $\mathcal{C}$, which are both of order unity. Later it was found that they might depend weakly on the exact geometry of the flow. Thus they have to be determined for each fork and each flow geometry separately. As their values are not essential to any of the following experiments, they will not be discussed here anymore and the reader will be directed to other publications for more details [18].

Now, the model was successfully tested in gases at room temperature, but will it hold in liquids and low temperatures? Another test was performed

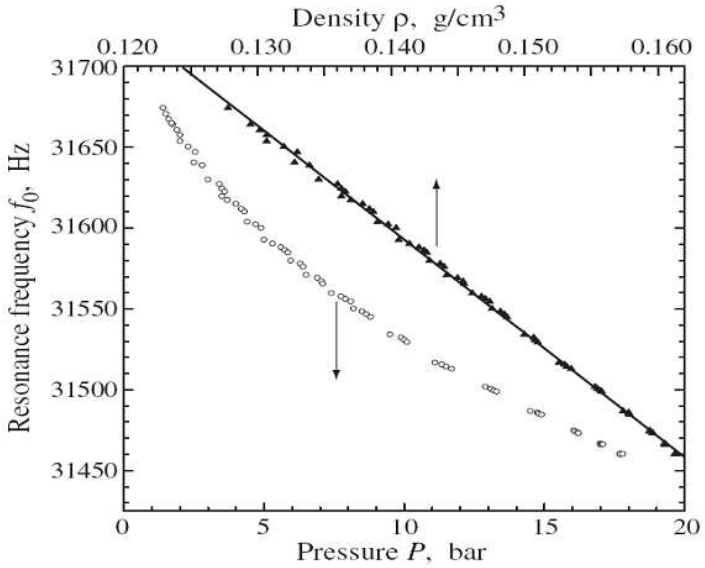

Figure 6.2: The resonant frequency of the standard 32 kHz fork in liquid He I at 4.2 K plotted versus applied pressure and corresponding density of He I

to see if it is the case, this time in He I at 4.2 K in pressures again up to 30 bar. The only minor difference is, that this time, the pressure had to be recalculated into density for the comparison to be meaningful. This recalculation was performed using the HEPAK [21] software package, carrying a comprehensive set of data on Helium physical properties both above and below the lambda transition. The results of this test are summarized in Fig. 6.2, which again shows that the model is valid in cryogenic liquids as well and describes the behaviour of the fork sufficiently despite the neglections we made when deriving the simplified relations for the resonant frequency and linewidth from the fork equations 4.12 and 4.13.

As the next step we proved that the tuning fork can indeed generate and detect turbulent flows. The fork was again immersed in He I and the amplitude of the driving voltage was gradually increased, while the measurements of the resonant curves were performed giving the resonant frequency, linewidth and amplitude. As it is nicely shown in Fig. 6.3, the response of the fork changes with the increasing drive amplitude. It shifts towards lower frequencies, the width increases and at a certain point, it ceases to be of the Lorentzian form. It should be emphasized, that our experimental setup allows investigations over an extremely broad range of the driving voltage,

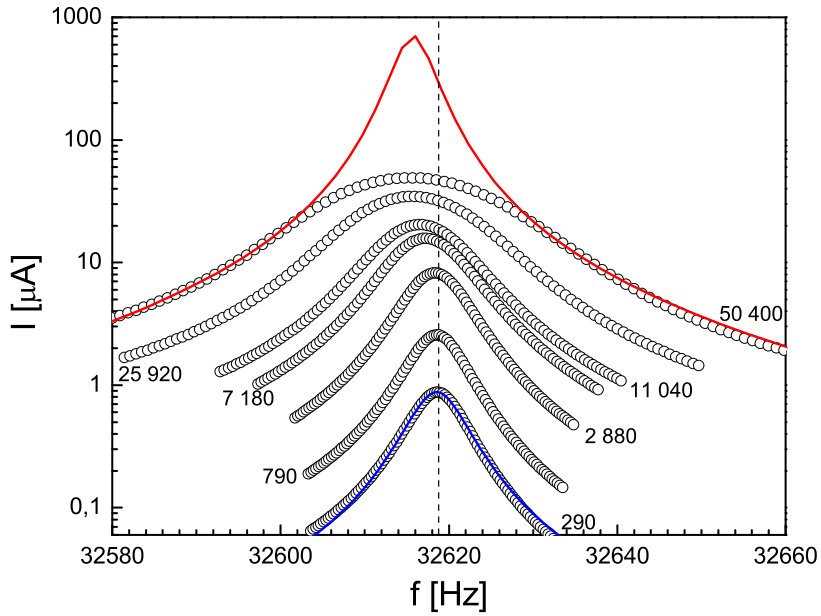

Figure 6.3: Resonant response of the fork at various drive amplitudes. The solid lines are Lorentzian curves. For details, see text.

exceeding seven orders of magnitude.

For a better understanding of the ongoing process, the dependence of $I(U)$, equivalent to $v(F)$ due to Equations 4.17 and 4.14, was plotted in logarithmic axes in Fig. 6.4. From this graph, is is immediately evident that two flow regions exist. In the first region (lowest drive amplitudes) the velocity is proportional to the force, hinting at the existence of a laminar flow, while in the second region, it assumes a square root dependence thus marking the turbulent drag regime and hinting at the existence of a turbulent flow. The insets also show that the transition from the laminar to the turbulent drag regime is marked by a pronounced decrease of the resonant frequency and an even stronger and more apparent increase of the linewidth. However, as these quantities are poorly defined for a non-Lorentzian resonance curve, it was decided that the relevant critical velocity for the transition to turbulence in classical fluids will be derived from the main graph itself as the velocity corresponding to the point of intersection of the lines fitted through the points deeply in the two separate regions.

Recently, visualization experiments on a vibrating rectangular beam (Fig. 6.5) immersed in water were performed as well, using the pH Baker tech-

nique, see [22] for details. Despite the fact that this setup is not precisely geometrically similar to the actual fork, it provides a good qualitative idea of what might be happening. The beam was firmly connected to a loudspeaker, which acted as a harmonic drive. Direct observation of the experiment showed that, at a certain critical velocity roughly corresponding to the one expected from the scaling, snake-like vortices began to form near the edges of the beam and were shedded away. This can be understood as an unequivocal proof that the phenomenon responsible for switching between linear and quadratic drag regimes is indeed the transition to turbulence.

6.1 Classical Fluids - Critical Velocity Scaling

In order to verify the scaling of the critical velocity $v_c \propto \sqrt{\nu\omega}$ in the widest possible range of viscosities and frequencies possible, experiments were performed using forks of different sizes and resonant frequencies, namely 32 kHz, 8 kHz and 4 kHz. These were immersed in various working fluids, ranging from the relatively viscous Helium gas at liquid Nitrogen temperature to liquid Helium just above T_λ, which is the classical fluid known for having the smallest kinematic viscosity.

The results on this scaling law are summarized in Fig. 6.6, where the observed critical velocity of the fork is plotted versus $\sqrt{\nu\omega}$ for all the mentioned experiments. From the graph, it is immediately evident that the scaling indeed holds for all the combinations of forks and fluids and the fit in the logarithmic inset found the exponent of the dependence to be 0.48 ± 0.04 which is in excellent agreement with the expected value of 0.5. As far as we know, this scaling law for oscillatory flows in the $R \gg \delta$ limit was proved for the first time. Therefore, its confirmation over several decades presents a valuable contribution to classical fluid dynamics.

6.2 Superfluid Helium

With the scaling of the critical velocity firmly established in classical fluids, the next step was to verify whether a similar scaling could be used for quantum fluids as well. The velocity scaling can be, in principle, used to determine an effective kinematic viscosity of the superfluid Helium attempting to describe it as a one-component quasiclassical fluid.

While this approach might be useful for describing several experiments,

we must bear in mind that it is only a simplification of the real problem, since He II is known to behave as if it consists of two distinct components with very different properties.

First, the force versus velocity dependence was measured for several temperatures and for different forks. Sample results are shown in Fig. 6.7 as well as the dependence for classical He I at 4.2 K. At the first sight, it seems that the dependence is the same as for classical fluids. If this were true, it would mean that in our experiments He II indeed behaves more or less like a quasiclassical one-component fluid. The velocity scaling mentioned above was therefore temporarily used to determine the effective kinematic viscosity and the obtained results were compared with the data from other experiments in He II, including those with vibrating grids [10] and second sound attenuation in thermal counterflow [23]. One of the outcomes of this preliminary analysis leads to a conclusion that He II should have a finite effective kinematic viscosity even in the $T \to 0$ limit. This contradicts a common notion that in this limit He II is entirely superfluid with zero viscosity.

We therefore performed a more thorough analysis, and it became evident that we could never describe the transition to turbulence in He II this way. After a closer look at Figure 6.7, it might be noticed that the force versus velocity dependence is not *exactly* the same as that for the classical fluids. Rather, another feature (difficult to see unaided in this graph) within the broad transition region is present as well. In order to see it clearly, we employed another approach based on the general equation for the drag force acting on a body in turbulent flow:

$$F_{turb} = \frac{1}{2} C_d S v^2. \tag{6.1}$$

From here, it is possible to evaluate the drag coefficient C_d based on the force versus velocity dependence. If C_d is plotted versus the velocity for a classical fluid across the transition region, it decreases monotonically for most body geometries to a constant value of order unity, which signifies the turbulent drag regime. However, when we plot C_d calculated for the vibrating forks from data acquired at various temperatures, we find a different behaviour, which is especially pronounced at the lowest temperatures near 1.3 K. It displays the laminar part, where the drag is due to the viscous normal fluid only, and then past a sharp minimum C_d increases again and displays a broad maximum, above which it gradually becomes constant as in the classical case. See Fig. 6.8 for a detailed picture of the discovered

dependence.

This complex dependence can hardly be explained by a single transition to turbulence in any hypothetical quasiclassical fluid. We are therefore left to conclude that perhaps two separate transitions actually occur - one in the normal component and one in the superfluid component. On first approximation, we may consider their velocity fields independent (although it is well known that when quantized vortices are present, the the components are coupled by the mutual friction force).

The idea of two separate transitions was further supported by consultations with other scientists, mainly Professor W.F. Vinen of the University of Birmingham. He proposed a phenomenological relation between the force (or the drag coefficient) and the velocity, assuming full independence of the two components of He II and the existence of two distinct transitions. Furthermore, the superfluid component does not contribute any laminar drag and the turbulent drag force due to the superfluid acts only above a critical velocity U_{cS}. The proposed equation takes the following form:

$$C_d = \frac{\alpha' \, 2 \, S/A \sqrt{2\pi f_0 \, \frac{\rho_n}{\rho} \, \nu}}{U} + \beta \frac{\rho_n}{\rho} + \gamma \left(1 - \frac{\rho_n}{\rho}\right) \Phi(U - U_{cS}) \left[\frac{(U - U_{cS})^2}{\epsilon + (U - U_{cS})^2}\right] \tag{6.2}$$

where Φ is the Heaviside step function, α', β, and γ are unknown numerical coefficients and the terms on the RHS describe the laminar drag of the normal component, the turbulent drag of the normal component and the turbulent drag of the superfluid component, respectively.

Equation 6.2 was used to fit our drag coefficient versus velocity data (again see Fig. 6.8) and to determine the critical velocity in the superfluid component, U_{cs}. The critical velocity of the normal component, U_{cN} was determined the same way as for classical fluids. This is justified under the assumption that the normal component behaves exactly like a classical viscous fluid.

The critical velocities for both the normal and the superfluid components for the 32 kHz fork are plotted versus the temperature in Fig. 6.9. Data obtained using forks vibrating at other frequencies was added to this picture, too. We show the critical velocities of the normal component as measured (at the frequency of the particular fork) as well as multiplied by the square root of the appropriate frequency ratio, in accordance with the proved $v_c \propto \sqrt{\nu\omega}$ scaling. This multiplication was done in order to check whether or not the

measured critical velocities of the normal fluid would collapse to a single temperature dependence. From Fig. 6.9 it can be seen that this is indeed the case. On the other hand, quite surprisingly, no dependence of the critical velocity of the superfluid component on the frequency of the oscillating fork was found.

As it is evident from Fig. 6.9, the re-scaled critical velocities of the normal component fall all above the critical velocities of the superfluid component. If all the assumptions used in this approach are true, and therefore our results are valid, it ought to be possible to find such a temperature and frequency at which the two critical velocities will be equal and a crossover in the C_d dependence should occur, since at lower frequencies, the superfluid component will become turbulent at higher velocities than the normal component. The experimental verification of this crossover will certainly be one of the issues to be studied in the near future.

6.3 Cavitation

There is one more interesting phenomenon that was observed during the experiments in liquid Helium. When the drive of the fork was increased gradually, usually first the transition to turbulence occurred. However, when the drive reached another critical level, the central region of the resonant response of the fork broke down completely as it is illustrated in Fig. 6.10.

Since this kind of breakdown was observed only in liquids and at the highest fork velocities achievable in our experiment, the only viable explanation is the cavitation process - local creation of a gaseous phase within the volume of the liquid. It should be noted that since evaporation is a first order phase transition, we must keep in mind that cavitation does not occur at the temperature and pressure corresponding to the saturated vapour pressure curve (SVP), but at a lower pressure, because the liquid can be "superheated". The term cavitation technically means that the nucleation line is crossed in the direction of the pressure axis, while (volume) boiling means reaching SVP in the direction of the temperature axis, see Fig. 6.11.

The breakdown of the fork's response was used to determine the critical cavitation velocity as the highest point that still lies on the original Lorentzian-like curve. When the cavitation velocity was plotted versus temperature (see Fig. 6.12), a pronounced almost step-like increase was observed close below the lambda point. The cavitation velocity in He II was three to four times larger then that in He I. It should be stressed that within the

framework of the standard nucleation model presented, e.g., in [24], there is no reason for this increase to occur.

Comparing our temperature dependence with [25] and [26], it was found that other experiments exhibit a similar, almost step-like increase in the vicinity of the lambda point. In these experiments, the negative pressure was produced by a piezoelectric oscillator of hemispherical shape emitting pressure waves. Thanks to constructive interference, these were amplified greatly in the center of the hemisphere. During the negative pressure swing, cavitation occurred. As it was pointed out, there should be no reason for any step-like increase around T_λ, so why is it observed?

A plausible explanation would be that during the measurements in He I, the fluid was also overheated locally, by the power dissipated by the oscillating fork, or by the power transmitted by the amplified pressure wave. Therefore, what probably happened, was that the nucleation line was not crossed in the direction of the pressure axis, but rather at a large angle to it (see again Fig. 6.11). If the thermal effects were significant, this process would distort the observed temperature dependence. As the heat transport efficiency in He I and He II differs by several orders of magnitude, the consequences of the above mentioned heating processes are very different above and below the superfluid transition. When the heat conductivity of He I is considered disregarding any convective flows, significant local overheating of the fluid in the vicinity of the vibrating quartz fork of the order of several K can be produced quite easily. However, in He II, local overheating is hardly possible. With the typical power dissipated by the fork, only a small counterflow velocity of order 1 cm/s is needed to carry the heat away from the fork, which means that almost no temperature gradient is created in the fluid. Furthermore, at the temperatures corresponding to He II, the nucleation line is already almost horizontal, meaning that the critical cavitation pressure depends on temperature weakly. Therefore, the nucleation line would be likely crossed in the direction of the pressure axis and a true cavitation velocity (or pressure) would be measured.

We must ask, however, do we really observe cavitation? Is not the breakdown caused by boiling instead? According to the Bernoulli equation, the pressure is indeed lowered in the vicinity of the moving fork, especially in the regions of high flow velocities near the sharp edges of the fork, where the flow velocity is enhanced strongly compared to the velocity of the fork itself. Therefore it seems, that at least in He II, where overheating can be neglected, true cavitation is most likely observed.

Strictly speaking, the Bernoulli equation describing the whole volume of the liquid generally holds only for stationary and potential flows, while the flow we are discussing is periodic and most likely turbulent. Therefore it was necessary to determine, if the Bernoulli equation can be at all used in our case. This was done by measuring the dependence of the cavitation velocity on an externally applied overpressure. The discovered dependence was approximately of the form $p \propto v^2$ as shown in Fig. 6.13. Since the square root dependence is in accord with the Bernoulli equation, it was inferred that it can perhaps be used to semi-qualitatively describe even the complicated turbulent flow.

Our critical velocity of the fork established for zero overpressure in He II corresponds to a negative change in local pressure of the order of 250 Pa. This is much lower than the results of other experiments, such as [25], where negative pressures of the order of several bar were found. This seems a large discrepancy, but there is a number of possible explanations. At first, we had thought that we measured heterogeneous cavitation, while the above mentioned experiments dealt with homogeneous cavitation far away from walls, but this idea had severe flaws. Since liquid Helium is actually the purest substance achievable, as at LHe temperatures all other elements are frozen solid, and since He II wets any surface ideally (perhaps with the exception of Cesium), it seemed inevitable to conclude that even in our experiments homogeneous cavitation most likely occurs.

Presently, we think that the discrepancy arises form the enhancement of flow velocities near the sharp edges of the fork (or from various excrescences at its surface). The velocity we measured was the amplitude of the velocity of the fork, but due to the hydrodynamic enhancement, the fluid near the edges moves much faster than the fork itself. To explain the enormous differences in the observed pressure (about three orders of magnitude), an enhancement factor of about 30 would be necessary. That is not as unfeasible as it might seem, because the ratio of the typical dimension of the fork (about $200 - 400$ μm) to the surface roughness, and therefore to the "radius of curvature" at the corners (typically about a few microns, see micrographs in Chapter 4) is roughly of the same order. Strictly speaking, our data do not therefore allow us to conclude with certainty, whether the observed cavitation is heterogeneous or homogeneous in nature.

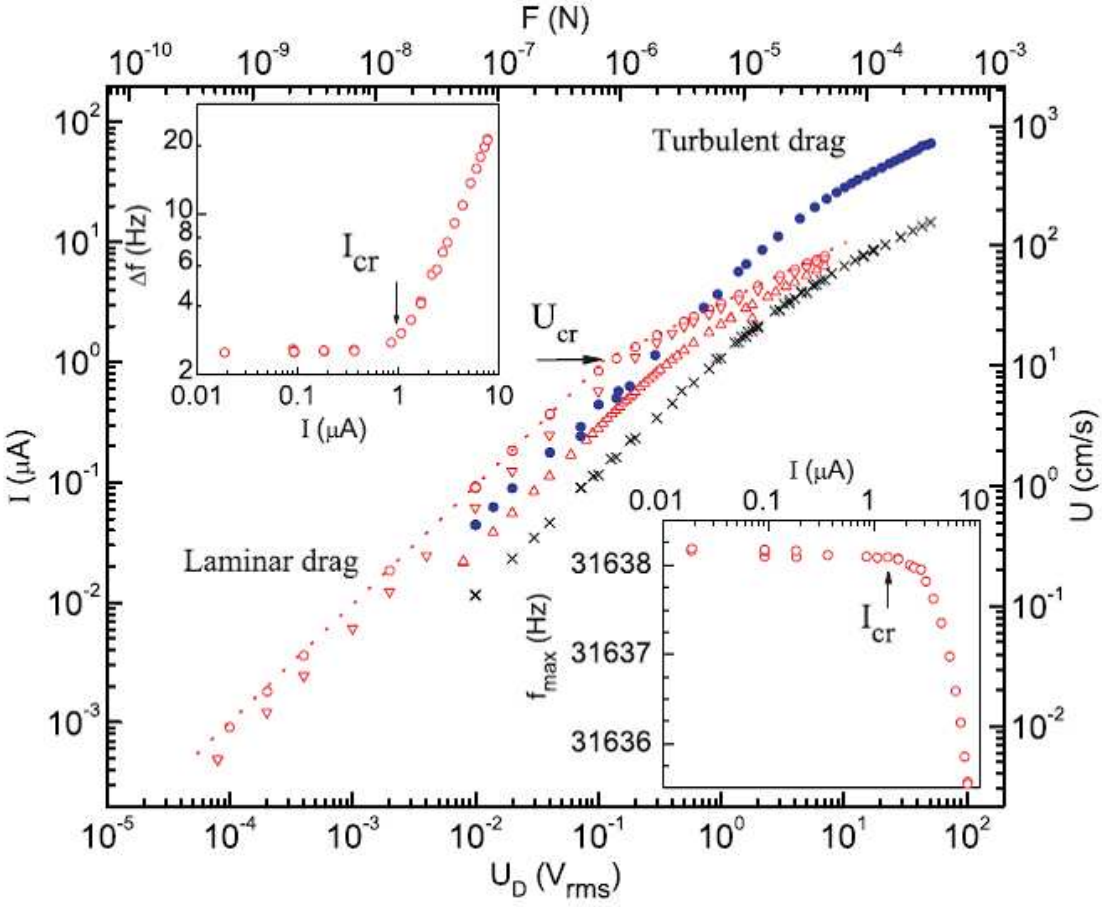

Figure 6.4: Transition from laminar to turbulent drag regime as detected by the 32 kHz vibrating quartz fork in He I at 4.2 K and 18.6 bar (×), in He II at SVP at 1.37 K (○), 1.61 K (▽), 2.06 K (△) and in gaseous helium at 78 K and 10.05 bar (•). For conversion of measured electrical quantities U_D and I to F and U, see [18]. The insets show the width Δf of the in-phase resonance response (top) and the frequency of maximum response f_{max} (bottom) versus measured current; both being constant in a linear regime. Increase of Δf and decrease of f_{max} indicate an onset of the turbulent drag regime.

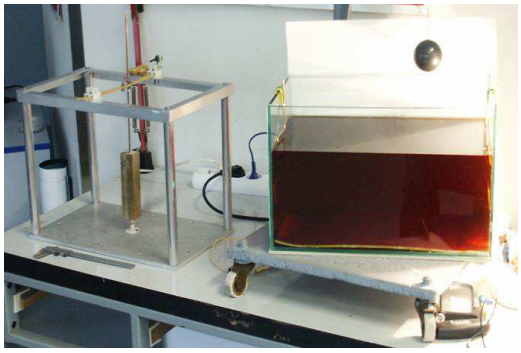

Figure 6.5: The beam and the Baker solution used for flow visualization

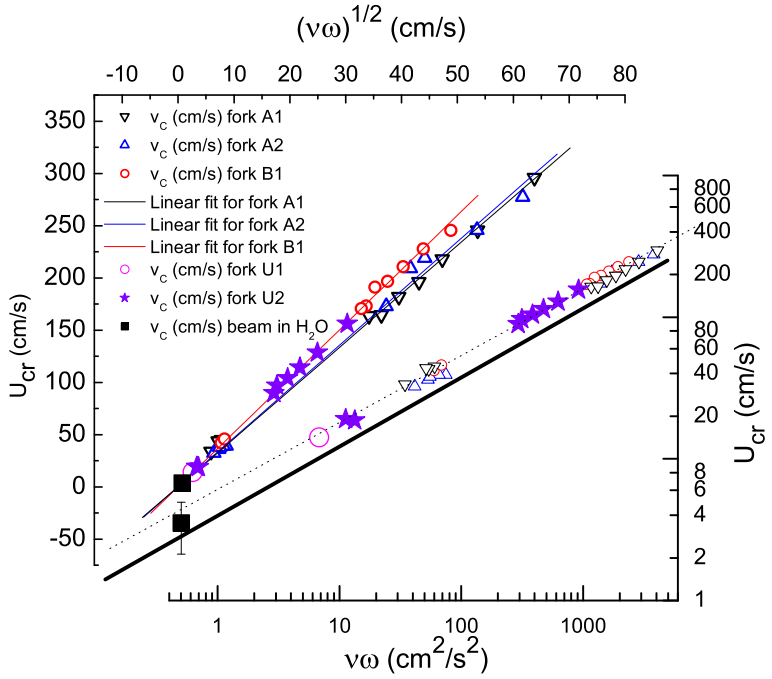

Figure 6.6: The critical velocity at which transition from laminar to turbulent drag occurs for five different forks A1, A2, B1, U1 and U2 in classical fluids (data points obtained using He I in the temperature range $2.2 < T < 4.2$ K and He gas at 78 K at ambient and elevated pressure up to 30 bar plotted versus $\sqrt{\nu\omega}$). The solid lines represent the best linear fit that includes the origin(top). This scaling is confirmed by comparison with the fixed solid line in the logarithmic plot (bottom); the fitted power law for all forks yields 0.48 ± 0.04. The black square point has been obtained with the rectangular brass beam using the pH Baker flow visualisation technique.

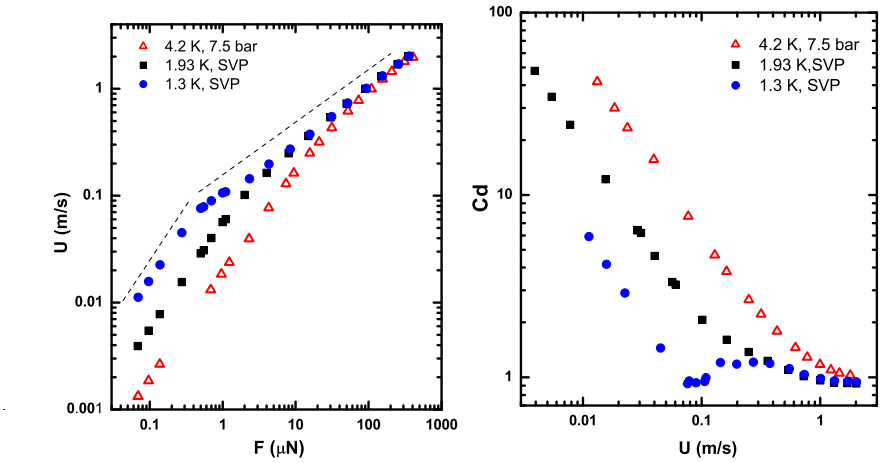

Figure 6.7: Left panel: Transition from laminar to turbulent flow of He II as detected by vibrating quartz fork in He I and He II at three temperatures as indicated. At low drive level (in laminar regime) the measured velocity is a linear function of the applied drive; around its critical value a crossover to a turbulent regime occurs, characterized by a quadratic driving force versus velocity dependence. Right panel: The plot of the drag coefficient versus the velocity of the fork clearly shows that in a classical fluid (He I) there is one gradual change towards its constant value well above the transition; while in He II there are two separate transitions in the superfluid and in the normal fluid, clearly displayed far enough below the T_λ. For details, see text.

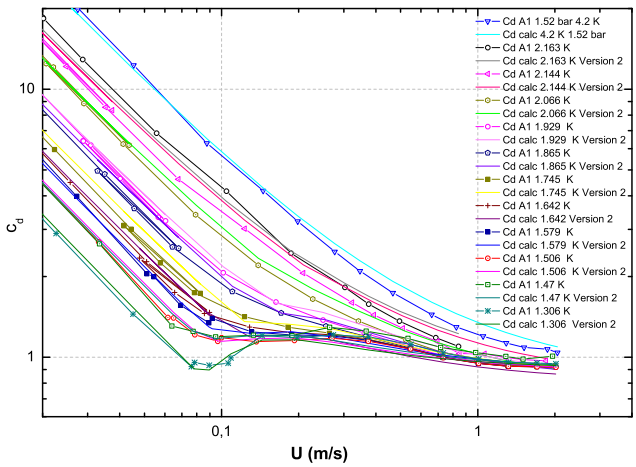

Figure 6.8: Detailed view of the drag coefficient versus velocity as measured in He I and He II at various temperatures. The solid lines are fits using Eq. 6.2. A detailed description can be found in the text.

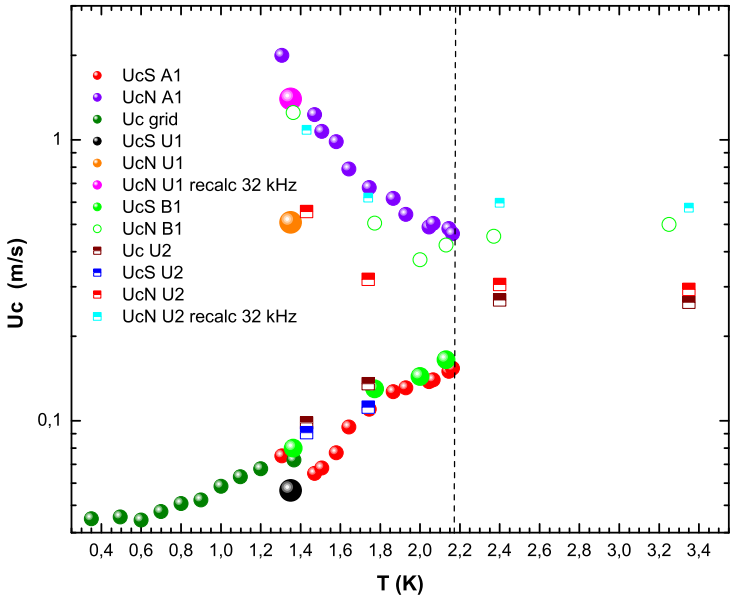

Figure 6.9: Critical velocities of the normal, U_{cN} and superfluid, U_{cS}, components obtained using Eq. 6.2 for various forks are plotted versus temperature. U_{cS} is always plotted as it was measured, since no frequency dependence was found, while for forks vibrating at other frequencies then 32 kHz, U_{cN} was plotted twice - once as measured and once after multiplying it according to the scaling proved for classical fluids, which is obviously the case of the normal component of He II too. Velocities measured above T_λ were obtained by the same method used in the previous section dealing with classical fluids and He I as such. For comparison, the critical velocities for fork U2 are plotted when evaluated both ways, U_c $U2$ was calculated as for purely classical fluids, while U_{cN} $U2$ and U_{cS} $U2$ were calculated according to Eq. 6.2.

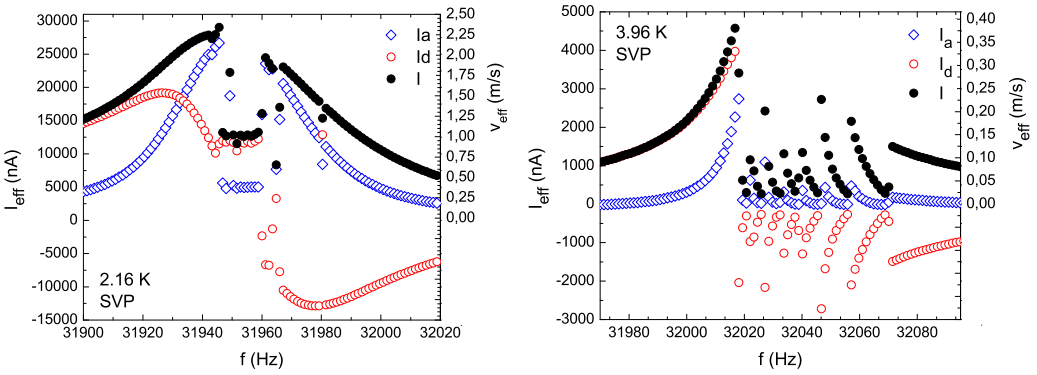

Figure 6.10: Broken responses of the tuning fork indicating cavitation

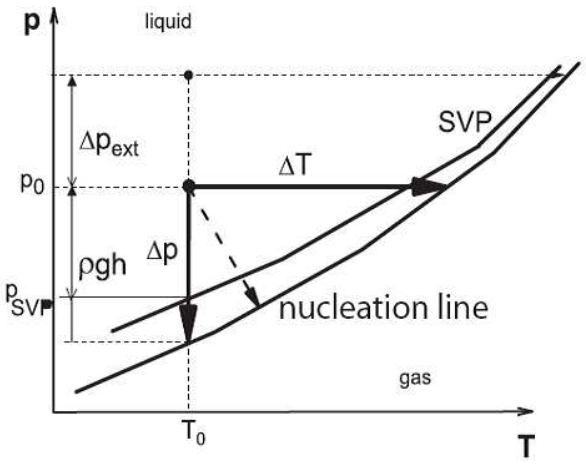

Figure 6.11: A detail of the He phase diagram showing both the SVP curve and the nucleation line, illustrating pure cavitation (vertical arrow) and boiling (horizontal arrow). Here, we assume that the fork is placed at the depth h below the Helium level (if an external overpressure Δp_{ext} were applied, the point would be shifted further upwards). For the vibrating quartz fork, the observed phenomenon is most likely a combination of both of these processes as schematically shown by the tilted broken arrow.

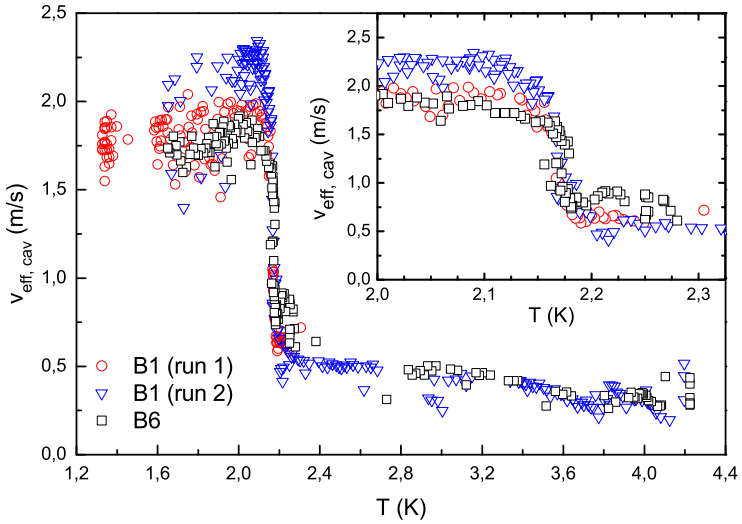

Figure 6.12: The critical cavitation velocity depending on temperature. The inset shows a detailed view of the vicinity of the superfluid transition.

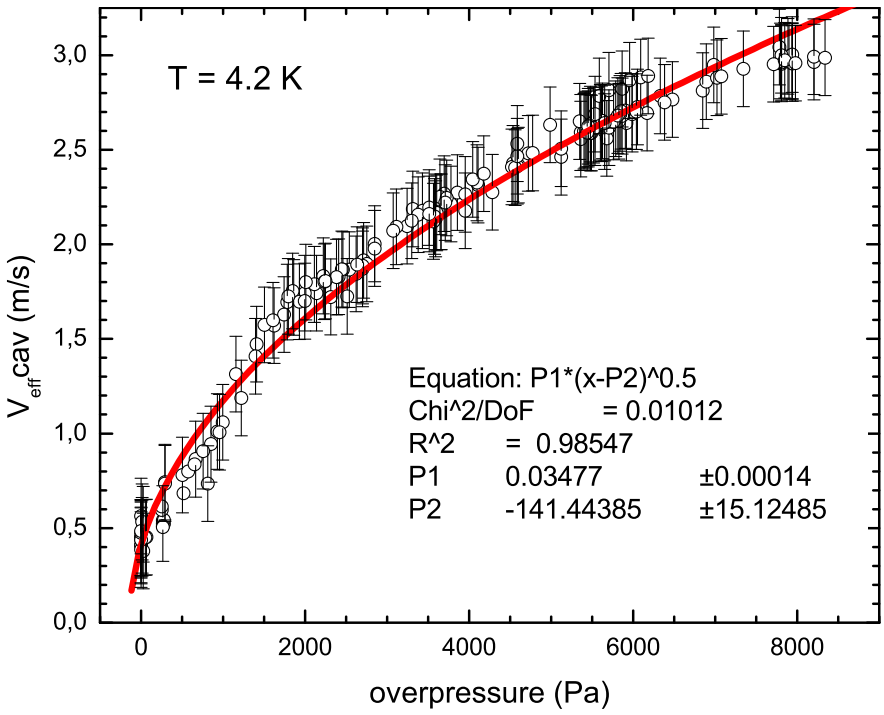

Figure 6.13: Dependece of the critical cavitation velocity on the applied overpressure at 4.2 K. The solid red line is a fit using the Bernoulli equation with the stated parameters.

Chapter 7

Conclusions

During the work on this Thesis, the ability of the quartz tuning forks to generate and detect flows in cryogenic liquids was tested. The forks proved to be cheap, widely available, simple to use, install and still very sensitive detectors of fluid properties. Furthermore, it was shown that they can be used to detect the transition to turbulence as well as other interesting phenomena such as cavitation in cryogenic liquid Helium.

The hydrodynamic model of the tuning fork was put forward and tested successfully in classical fluids. Due to the extremely wide range of kinematic viscosities of various Helium fluids, it was possible to verify the scaling of the critical velocity for the transition from the laminar to the turbulent drag regime in boundary layer flows near bodies oscillating at sufficiently high frequencies.

When immersed in quantum fluids, the quartz tuning fork serves equally well as a detector of fluid properties and of the transition to turbulence. It was found, however, that in this type of flow, two different turbulent states may exist and that the transition to turbulence is rather complex, as the normal and the superfluid component becomes turbulent at different velocities. The detailed structure of the transition from the laminar to the turbulent drag regime and the corresponding flow phase diagram will be subject of further studies, as will be other applications of the quartz tuning fork in cryogenic fluid dynamics including, e.g., the detection of counterflow turbulence.

The quartz tuning fork has also been used to detect cavitation in Helium liquids. The interpretation of the acquired results does present a considerable challenge. In particular, it was shown that thermal effects are essential for

the interpretation of the cavitation results obtained in both He I and He II.

The results discussed herein have been acquired owing to the common efforts of the members of the superfluidity group within the Joint Low Temperature Laboratory, established between the Faculty of Mathematics and Physics of the Charles University in Prague and the Institute of Physics of the Academy of Sciences of the Czech Republic, Prague. This research is supported by GAUK under the grant no. 7953/2007: *Study of Helium Superflow Due to a Vibrating Quartz Crystal*, awarded to the author for the years 2007-2009. The results have been published (or submitted for publication) in recognized scientific journals. They were also presented by the author in two talks: i) *The Flow Properties of LHe, Quantum Turbulence and Cavitation*, at the seminar of the Department of Low Temperature Physics, ii) *Quartz Tuning Forks as Low Temperature Sensors*, at an intensive course called Contemporary Problems of Low Temperature Physics in Pec pod Snezkou, May 6th - 10th, 2007. Other members of the Laboratory have presented them at several conferences, both in the Czech Republic and abroad (see the attached List of Publications).

In summary, the quartz tuning fork has proved to be an extremely useful tool for generating and probing cryogenic flows and will certainly continue to be used in future experiments as a full and valid member of the family of various oscillating objects - cornerstone devices of cryogenic fluid dynamics research since its very beginning.

Bibliography

[1] R. J. Donnelly, C. F. Barenghi (1998): J. Phys. Chem. Data **27** 1217.

[2] R.S. Šafrata et al. (1998): *Fyzika nízkých teplot*, Matfyzpress, Praha.

[3] J. Formánek (2004): *Úvod do kvantové teorie I.,II.*, Academia, Praha.

[4] R.J. Donnelly (1991): *Quantized vortices in Helium II*, Cambridge University Press, Cambridge.

[5] L.D. Landau, E.M. Lifshitz (1987): *Fluid Mechanics*, Pergamon Press, Oxford, UK.

[6] L.M. Milne-Thomson (1996): *Theoretical hydrodynamics* (Dover Publications, New York.

[7] D.R. Tilley, J. Tilley (1986): *Superfluidity and Superconductivity*, Adam Hilder, Ltd., Bristol

[8] M. Niemetz, et al. (2002): J. Low Temp. Phys. **126**, 287 (2002); W. Schoepe (2004): Phys. Rev. Lett. **92**, 095301 – electrically driven magnetically levitated oscillating sphere in ^{4}He-II.

[9] E.N. Martinez, et al. (1990): Am. J. Phys. **58**, 1163.

[10] H.A. Nichol, et al. (2004):, Phys. Rev. Lett. **92**, 244501 and Phys. Rev. E **70**, 056307 – electrically driven oscillating grid in ^{4}He-II.

[11] D.I. Bradley, et al. (2005): Phys. Rev. Lett. **95**, 035302 and (2006): *ibid.* **96**, 035301.

[12] H. Yano, et al. (2005): J. Low Temp. Phys. **138**, 561 – vibrating wire resonator in ^{4}He-II.

[13] D.I. Bradley (2000): Phys. Rev. Lett. **84**, 1252.

[14] J. Martikainen, et al. (2002): J. Low Temp. Phys. **126**, 139 – vibrating wire resonator in ^{3}He – ^{4}He solution.

[15] J. Rychen, et al. (1965): Rev. Sci. Instr. **71**. (2000).

[16] D.O. Clubb, et al. (2004): J. Low Temp. Phys. **136**, 1.

[17] K. Karrai, lecture notes (2000) at http://www.nano.physik.uni-muenchen.de/publikationen/preprints/p-00-03_Karrai.pdf.

[18] R. Blaauwgeers et al. (2007): *Quartz Tuning Fork: Thermometer, Pressure- and Viscometer for Helium Liquids*, J. Low Temp. Physics **146** No. 5/6 537-562.

[19] M. Blazkova, D. Schmoranzer, L Skrbek (2007): *Transition from Laminar to Turbulent drag Regime in Flow due to a Vibrating Quartz Fork*, Phys. Rev. E **75**, 025302.

[20] L. Skrbek et al. (2006): *Transition to turbulence of flow due to a vibrating quartz fork in classical and quantum fluids*, 59-th Annual DFD APS meeting, Tampa Bay, Florida, November 19-21, Bulletin of American Physical Society 51, No 9, p.100

[21] V.D. Arp, R.C. McCarty (1998): The Properties of Critical Helium Gas (Technical Report, Univ. Oregon; R.D. McCarty (1972): Thermophysical Properties of Helium-4 from 2 to 1500 K with Pressures to 1000 atm, (Technical Note 631, National Bureau of Standards, Gaithersburg, Maryland.

[22] D.J. Baker (1966): Journal of Fluid Mechanics **26**, part 3, p. 573-575.

[23] T.V. Chagovets et al. (2007): Phys. Rev. E **76**, 027301.

[24] S. Balibar (2002): J. Low Temp. Phys. **129**, 363.

[25] F. Caupin, et al. (2003): Physica B **329-333**, 356.

[26] R.D. Finch, et al. (1964): Phys. Rev. **134**, A 1425.

APPENDIX A - List of Publications

Original journal papers

1. R. Blaauwgeers, M. Blazkova, M. Clovecko, V.B. Eltsov, R. de Graaf, J. Hosio, M. Krusius, D. Schmoranzer,W. Schoepe, L. Skrbek, P. Skyba, R.E. Solntsev, and D.E. Zmeev: *Quartz Tuning Fork: Thermometer, Pressure- and Viscometer for Helium Liquids*, J. Low Temp. Physics 146 No5/6 (2007) 537-562
2. M. Blazkova, D. Schmoranzer, L Skrbek: *Transition from Laminar to Turbulent drag Regime in Flow due to a Vibrating Quartz Fork*, Phys. Rev. E 75, 025302 (2007)
3. M. Blažková, M. Človečko, V.B. Eltsov, E. Gažo, R. de Graf, J.J. Hosio, M. Krusius, D. Schmoranzer, L. Skrbek, P. Skyba, R.E. Solntsev: *Vibrating Quartz Fork - a Tool for Cryogenic Helium Research*, submitted to J. Low Temp. Physics
4. L. Skrbek, M. Blažková, T.V. Chagovets, M. Rotter, D. Schmoranzer: *Cavitation in Liquid Helium Observed in a Flow Due to a Vibrating Quartz Fork*, submitted to J. Low Temp. Physics

Conference Proceedings

1. M. Blažková, D. Schmoranzer, M. Šindler and L. Skrbek: *Transition from Laminar To Turbulent Drag in Flow Due To a Vibrating Quartz Fork in Normal and Superfluid Helium*, Proc. Of the Colloquium Fluid Dynamics (Kolokvium Dynamika tekutin 2006), ISBN 80-87012-01-1, Editors P. Jonáš, V. Uruba, Prague, Institute of Thermodynamics, October 25-27, 2006, p. 13-16
2. L. Skrbek, M. Blazkova, D. Schmoranzer: *Transition to turbulence of flow due to a vibrating quartz fork in classical and quantum fluids*, 59-th Annual DFD APS meeting, Tampa Bay, Florida, November 19-21, Bulletin of American Physical Society 51, No 9, p.100